Applications of Novel Silicon and Aluminum Based Substrates for the Surface-Enhanced Spectroscopies: SERS and SEF

by

Alisher Sultangaziev

A thesis submitted in conformity with the requirements
for the degree of Master of Science in Chemistry
Graduate department of Chemistry
School of Sciences and Humanities
Nazarbayev University
04/2021

Acknowledgments

First and foremost, I would like to thank my supervisor, Professor Rostislav Bukasov, for providing me with the opportunity to learn about Raman spectroscopy and participate in several research projects during my undergraduate studies, as well as the opportunity to work on this very exciting project for my Master's degree. Furthermore, I want to thank him for the guidance and support throughout the entire study, as well as for being an outstanding mentor to me. I sincerely thank him for his assistance and understanding over the last four years.

In addition, I would like to thank the many present and former members of our research group who have assisted me with this research. I would like to thank Alisher Rapikov and Zhanar Kunushpayeva for their invaluable assistance with the immunoassays, Raman measurements, and cell labeling. I would also like to thank them for their assistance with the SEM and AFM measurements. I would also like to thank undergraduate students Aktilek Akhmetova and Dina Dossym for their help with Raman measurements and immunoassay preparation. This work would not have been completed without the assistance of my coworkers.

Secondly, I want to thank the Core facility and particularly Laura Khamkhash for providing access, maintenance, and assistance with the operation of AFM, SEM, and Raman microscope. Also, I want to thank Professor. Olena Filchakova for the help in bacteria growth and toxicity experiment. In addition, I want to thank the faculty of the Chemistry department for their knowledge and guidance throughout my graduate and undergraduate studies. In particular, I want to thank Professor Haiyan Fan for her time as my advisor and for the help given during difficult times.

Finally, I'd like to express my appreciation and love for my family, especially my Mother. I'd like to thank her for all of her encouragement and support throughout my studies. I would not have made it without her.

Alisher Sultangaziyev

Abstract

This Master's thesis investigates the applicability of non-traditional substrates for surface-enhanced Raman spectroscopy and surface-enhanced fluorescence. The use of silicon wafer for sandwich SERS immunoassay and aluminum foil for SEF in bacteria labeling with quantum dots were assessed.

Perhaps the first application of silicon wafer for sandwich immunoassay resulted in an analyte limit of detection of 30 pM with a dynamic range of 0.03-4 nM. In comparison to gold film, it produced a signal intensity that was one order of magnitude lower, which was compensated for by a significantly lower standard deviation in the blank signal.

The experiment on *E.coli* bacteria labeled with CdSeS/ZnS composite quantum dots yielded a high level of surface enhancement for all three substrates including uncommon aluminum foil and aluminum film. When the laser excitation source was changed, the results remained consistent, and there was a clear distinction between labeled and unlabeled cells.

Overall, both silicon wafer and aluminum foil showed comparable results to conventional gold film and silver film substrates in different applications. Both of these substrates were found to be less expensive and produced more reproducible results than conventional substrates.

Table of Contents

List of figures

List of tables

List of abbreviations

AFM – atomic force microscopy

Ag-FON – silver film on nanosphere

AU – arbitrary units

BG - background

BSA – bovine serum albumin

CCD – charge-coupled device

cps – counts per second

EDS – energy dispersive X-ray spectroscopy

EF – enhancement factor

ERL – extrinsic Raman label

LOD – limit of detection

LOQ – limit of quantification

LSPR – localized surface plasmon resonance

NBARI – normalized blank-adjusted Raman intensity

NP - nanoparticle

MEF – metal-enhanced fluorescence

PBS – phosphate-buffered saline

QD – quantum dot

RSD – relative standard deviation

SEF – surface-enhanced fluorescence

SERS – surface-enhanced Raman spectroscopy

STDEV – standard deviation

1.0 Introduction

1.1 Surface-Enhanced Raman Spectroscopy (SERS)

Since its discovery in 1974 and identification in 1977,[1-2] surface-enhanced Raman spectroscopy (SERS) has become a powerful and popular analytical technique with more than thirty thousand academic papers published in the last decade only. This level of attraction for SERS stems from its high sensitivity, non-destructive nature, speed, and ability for label-free detection with strong potential for multiplexing.[3] Because of these and other advantages, SERS has found applications in molecular biology,[4-6] biomedicine[7-9], and environmental science[10], and showcasing even single-molecule detection.[11-14] However, various factors can affect the reproducibility of SERS measurements, such as pH, the degree of nanoparticle aggregation, temperature, substrate composition, etc. [15] Therefore, the research on these effects on the enhancement of the SERS signal and the development of new SERS instruments and substrates is needed to make this analytical technique more widespread.

The core theory of SERS is based on the enhancement of Raman scattering, which is very weak in and of itself. Raman signal is generated when photons strike the matter and produce inelastic scattering. This photon scattering can be significantly amplified by placing the matter near the surface of plasmonic nanostructures via two different mechanisms: (a) an electromagnetic enhancement and (b) a chemical enhancement. The relationship between normal Raman signal and SERS signal can be seen in the equation below, where P_{SERS} and P_{Raman} represent respective signal intensities and G_{SERS} denotes a combination of electromagnetic and chemicals enhancements.

$$P_{SERS} = G_{SERS}P_{Raman} = G_{SERS}^{Em}G_{SERS}^{Chem}P_{Raman} \quad (1)$$

Electromagnetic enhancement arises from the light-induced electric fields on the surface of particular nanostructures. These enhanced electric fields are generated when the incident light is in resonance with the oscillations of conduction electrons of the metal nanoparticle,

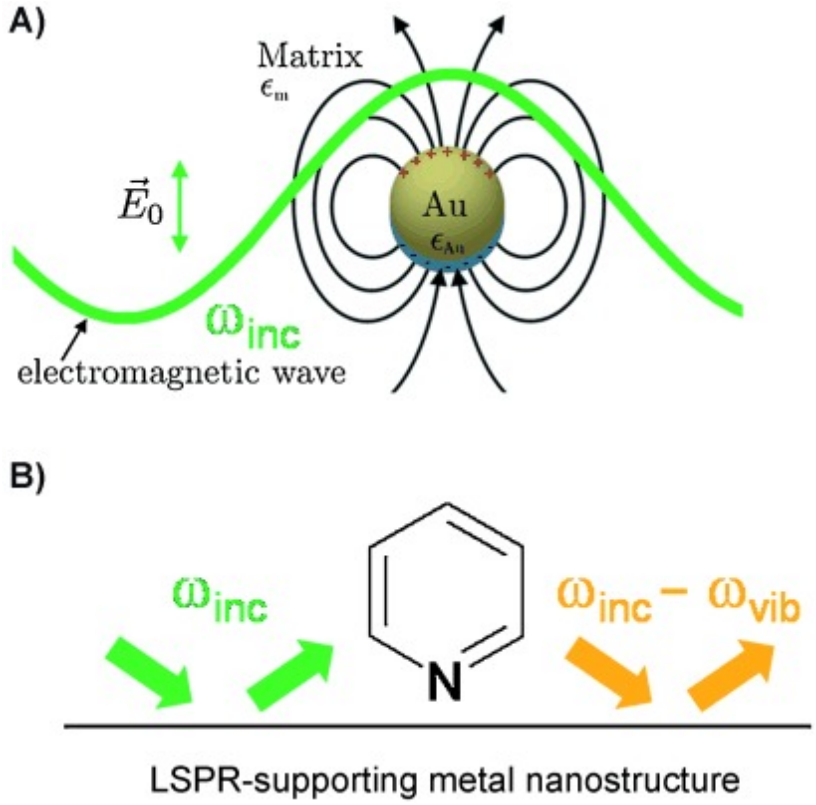

Figure 1. Electromagnetic enhancement in SERS. A) Excitation of a LSPR in gold nanoparticle. B) Both the "incoming" field (green arrows) and the "outgoing" field (orange arrows) are enhanced by LSPR-supporting metal nanostructure. Reprinted with permission from Schlucker[30], John Wiley and Sons.

which will make conduction electrons oscillate collectively. This optical phenomenon is called localized surface plasmon resonance (LSPR).[16] Electromagnetic enhancement increases the Raman scattering at least by the factor of 10^4 and as high as 10^{10}.[17-18] The schematic representation of this phenomena can be observed in Figure 1. This enhancement mechanism is dependent only on the configuration of a substrate with no regard for the analyte molecule. It can be seen more clearly in equation 2 for the single-molecule electromagnetic enhancement $|E^4|$ approximation, where $M_{Loc}^{Z}(\omega_L)$ and $M_{Loc}^{Z}(\omega_R)$ are the terms for the field enhancement generated by laser polarization either at the frequency of laser or Raman.[19]

$$G_{SERS}^{EM}(E^4) = M_{Loc}^{Z}(\omega_L)M_{Loc}^{Z}(\omega_R) = \left[\frac{E_{Loc}(\omega_L)}{E(\omega_L)}\right]^2 \left[\frac{E_{Loc}(\omega_R)}{E(\omega_R)}\right]^2 \quad (2)$$

On the other hand, chemical enhancement arouses from the localized electronic resonance of adsorbate or charge transfer resonance from the surface to metal nanoparticles and gives the enhancement of 10^2-10^4 order.[20] This phenomenon can be further explained by the following equation, where σ_k^{ads} and σ_k^{free} represent k-th order vibrational mode Raman frequencies of the free and adsorbed molecule.

$$G_{SERS}^{Chem} = \sigma_k^{ads}/\sigma_k^{free} \quad (3)$$

The combination of these two phenomena can produce signal enhancement levels as high as 10^{14} order of magnitude. However, the highest levels of signal enhancement can be achieved only in nanometer-sized junctions or gaps between plasmonic nanostructures or nanostructures and metal surfaces. These locations are called “hot spots” and their effect on signal enhancement is inversely proportional to the gap distance and can be well explained in the distances between 2-10 nm. However, when the gap distance goes below 1 nm, quantum effects like electron tunneling become more predominant, and strong enhancement of electromagnetic field can start affecting analyte and nanostructure.[21] Therefore, taking into consideration the nature of the SERS phenomenon we can clearly

state that the substrate and nanoparticle stability in terms of aggregation, particle metal oxide composition, surface chemistry, etc., plays an important part in their plasmonic properties and significantly affect SERS performance.[22]

The biggest contribution to this field was made by the group of Dr. Van Duyne, who is responsible for the discovery of the SERS effect.[1] Also, they were the first ones to find and characterize the effect of "hot spots", which is responsible for the majority of Raman signal enhancement in SERS.[23-24] Works of this group described not only the theoretical knowledge of SERS phenomena but also the synthesis and characterization of plasmonic nanostructures and their applications in diagnostics. For example, the development of a procedure for quick detection of highly dangerous anthrax spores.[25] By using self-developed and synthesized silver film over nanosphere (Ag-FON) substrate they detected safe *Bacillus subtilis* spores, which has a high resemblance to anthrax spores. With 11 minutes spent on the whole procedure, they were able to detect the number of analyte spores as low as 2.6×10^3. Also, they found that even one month old Ag-FON substrates can be successfully used for the detection of spores. Another seminal work of this group is about the in vivo detection of glucose concentration in rats through the skin.[26] They achieved it by implanting Ag-FON substrate functionalized by mixed self-assembly monolayer (SAM). Results showed that this system can accurately and reliably detect a low concentration of glucose (<80 mg/dL) with a root-mean-square error of prediction of 13.7 mg/dL and root-mean-square error of calibration of 3.6 mg/dL. And the sensor was operational for 17 days after implantation, which shows potential for further development of a human-oriented sensing system. In addition to the numerous research articles like these, the group of Dr. Van Duyne published numerous comprehensive reviews on SERS from both theoretical and practical perspectives.[20, 27-30]

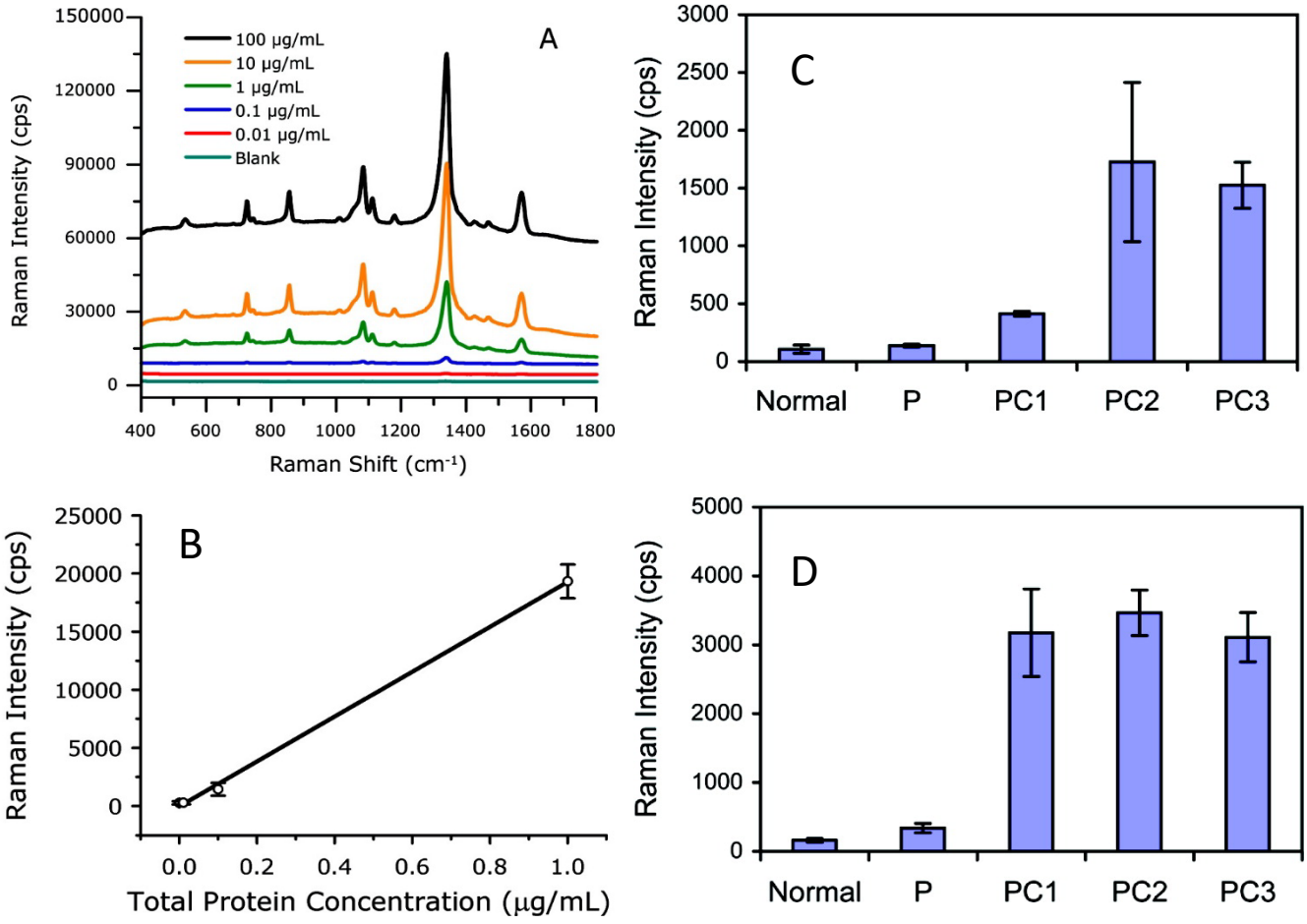

Figure 2. SERS-based assay for MUC4 in PBS buffer. A) SERS spectra at different cell lysate concentrations. B) Linear range of calibration curve. SERS detection of C) MUC4 and D) CA 19-9 in pooled sera from healthy and cancer patients (PC1, PC2, PC3). Adapted with permission from Wang et al.[32]. Copyright 2021 American Chemical Society.

Also, it is important to mention the seminal works of the Porter group for the application of SERS in immunoassays, which had a significant influence on this thesis project.[9, 31] One of the earlier examples of such work describes the detection of prostate-specific antigen (PSA) by using extrinsic Raman labels (ERLs) containing gold nanoparticles modified with Raman reporter and antibodies.[9] They achieved 1 pg/ml limit of detection (LOD) for PSA in human serum and 4 pg/ml limit of detection for PSA in bovine serum albumin solution. According to the authors, these values are lower than the operating range of the commercially available assays for PSA. Building on these findings, they performed the SERS immunoassay of the mucin protein MUC4 and cancer antigen CA19-9 for the early diagnosis of pancreatic cancer.[32] Results of the Raman measurement and subsequent calculations yielded LODs for MUC4 of 33 ng/ml and CA19-9 27 ng/ml. Also, analysis of clinical samples from pancreatic cancer patients produced significantly different results than samples from healthy patients for both MUC4 and CA 19-9 with $P<0.001$. These results can be observed in more detail in Figure 2. Thus, this diagnosis method has the potential for the detection of cancer biomarkers in real-life samples with better sensitivity than traditional methods of diagnosis. Overall, these research works represent only a fraction of prospects for SERS but can demonstrate its importance and capabilities as an analytical technique.

1.2 Surface-Enhanced Fluorescence (SEF)

Fluorescence spectroscopy has been an indispensable analytical instrument in biotechnology and medicine over the last 40 years. It detects molecules with moderate to high sensitivity quickly and reliably.[33] Nonetheless, improving the sensitivity of this technique is still highly desirable. This property of the fluorescence is usually limited by the quantum yield and fluorescence lifetime. The quantum yield (Q_0) determines the

efficiency of the fluorescence and demonstrates the ratio of photon emission against non-radiative decay:

$$Q_0 = \frac{\Gamma}{\Gamma + k_{nr} + k_q} \qquad (4)$$

Where Γ is the radiative decay rate of the fluorophore, which is the rate of photon emission. The terms k_{nr} and k_q depict the phenomena by which the fluorophore can return to the ground state: non-radiative decay and other quenching processes, respectively. And the fluorescence lifetime is described by the time fluorophore remains in the first singlet state on Jablonski diagram[34], and illustrated by the following equation:

$$\tau_0 = \frac{1}{\Gamma + k_{nr} + k_q} \qquad (5)$$

Usually, these parameters can be altered by changing the magnitude of the non-radiative decay and other quenching processes, as the radiative decay rate Γ is the constant value that depends on the extinction coefficient of the fluorophore.[35] However, by placing the fluorophore near the conducting metal surface or particle it is possible to change the radiative decay rate Γ and influence the quantum yield and fluorescence lifetime.[36]

The theoretical background behind the effects of the metal surfaces on fluorescence has been well studied and summarized in various articles and reviews.[37-39] It was found that two main effects are responsible for the change in the fluorescence in the proximity of the metal surface. The first one is the amplification of the incident light by the inner free electrons of the metal, which is called the "lightning rod effect".[40] This effect can be utilized to obtain localized enhancement of the fluorescence and to significantly increase the rate of excitation and intensity. The second effect is the increase in radiative decay rate through additional metal-induced radiative rate Γ_m. This term modifies equations 4 and 5 accordingly:

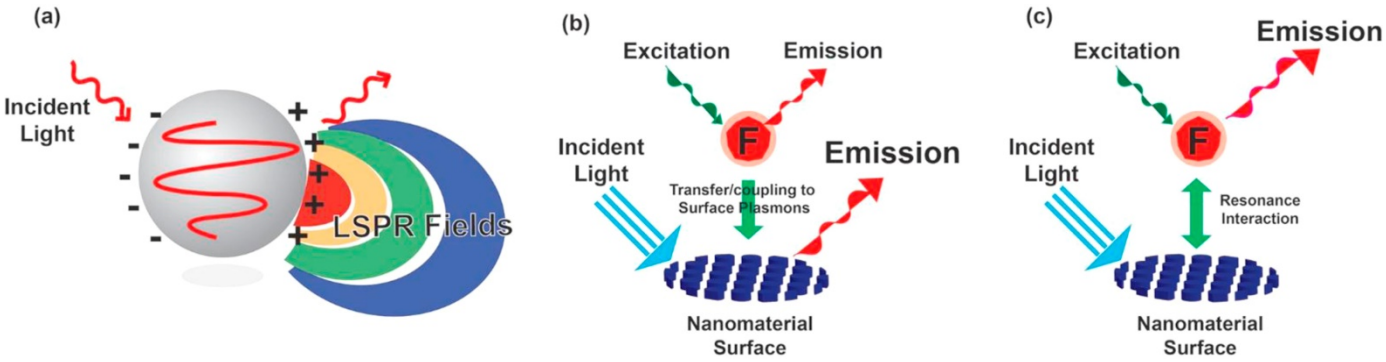

Figure 3. Mechanism of MEF. (a) Localized surface plasmon resonance (LSPR). (b) Plasmon-coupling effect. (c) Radiative decay engineering (RDE). Reprinted with permission from Jeong et al.[42], Elsevier B.V.

$$Q_m = \frac{\Gamma + \Gamma_m}{\Gamma + \Gamma_m + k_{nr} + k_q} \quad (6)$$

$$\tau_m = \frac{1}{\Gamma + \Gamma_m + k_{nr} + k_q} \quad (7)$$

So, the increase in quantum yield and decrease in fluorescence lifetime can be achieved by placing the fluorophore near the conducting metal surface or particle. The combination of these phenomena is called metal-enhanced fluorescence (MEF) or more broadly surface-enhanced fluorescence (SEF).[41-42] The schematic representation of this phenomenon can be observed in Figure 3. Thus, the choice of proper substrate for the SEF has a significant impact on the overall performance of this analytical technique.

Most of the development in the SEF area is based on the classic works of Lakowicz and Geddes group in the early 2000s.[43-45] They not only pioneered the SEF research area, but they also were one of the first to investigate the SEF potential of non-noble metals like aluminum. The first such work was published in 2007 and contained information about the use of novel aluminum nanostructured surfaces for MEF applications.[46] The substrate was synthesized by vacuum evaporation deposition on the surface of the quartz slide, with further modification by a 5 nm silica layer for the protection of the metal surface. This

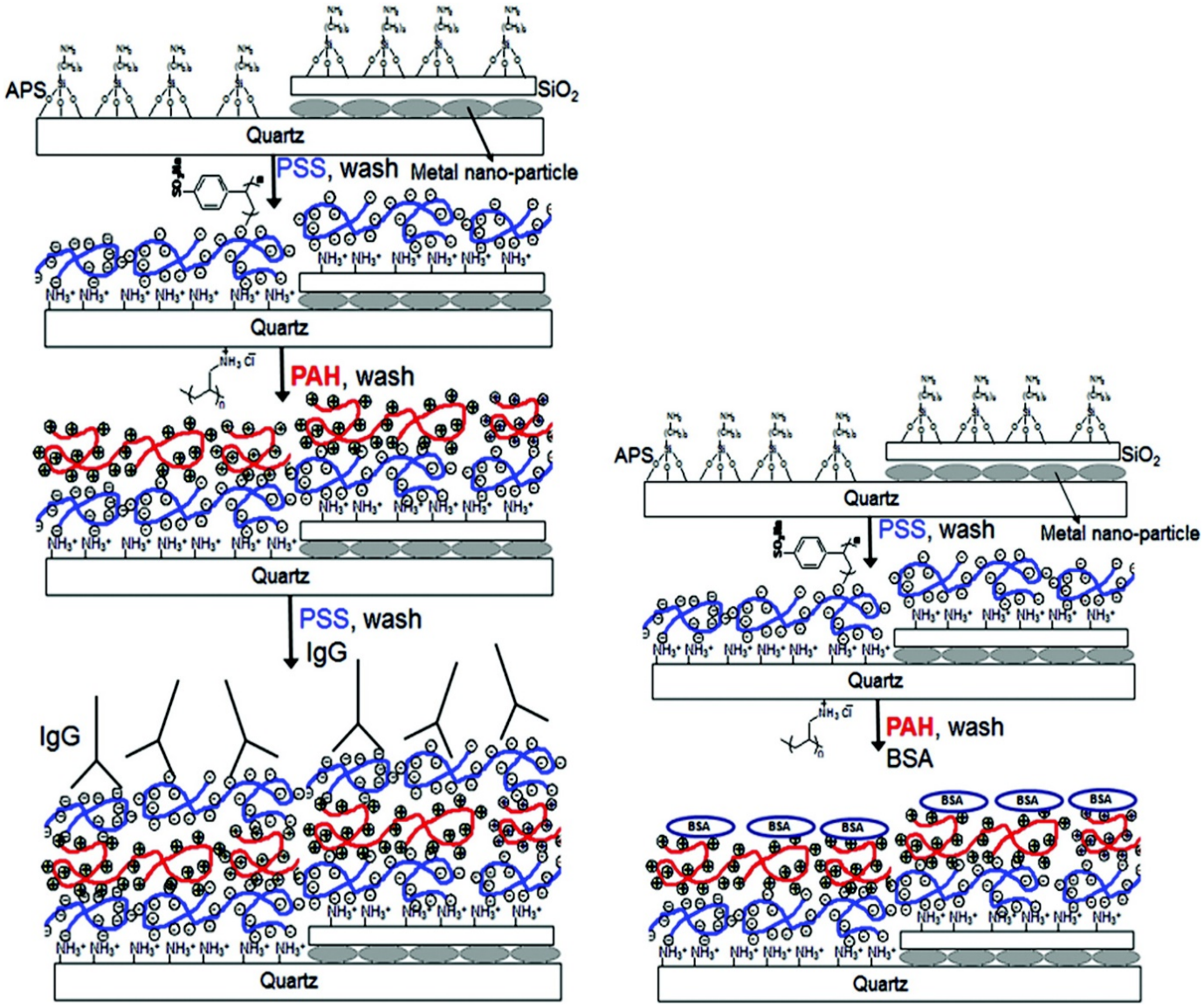

Figure 4. Schematic representation of assay procedure and layer-by-layer deposition. Reprinted with permission Akbay et al.[48] Copyright 2021 American Chemical Society.

substrate showed increased efficiency in the UV-blue spectral regime with two probes of choice, resulting in better fluorescence emission, lower fluorescence lifetimes, and greater photostability. With this, they paved a way for further studies on the use of aluminum substrates in MEF.

In the following years, the group of Dr. Lakowicz published several articles showcasing the potential of their novel aluminum substrate. In 2009, they observed an increase of intrinsic fluorescence from proteins due to the proximity of aluminum nanostructured surface.[47] The observed 14-fold increase in fluorescence intensity, as well as a 6-fold decrease in fluorescence lifetime in comparison with quartz substrates. Moreover, they were able to show the possible application for immunoassays by analyzing the binding of streptavidin to the surface of the modified aluminum nanostructure film. The most important part about this is they did not use any label molecules for the analyte. They built upon this successful presentation of the aluminum substrate, and in 2012 published an article on the effect of probe distance on the fluorescence intensity and lifetime by using the layer-by-layer technique.[48] By using this technique, they were able to precisely control the distance between the aluminum surface and the protein layer. The schematic representation of layer-by-layer deposition can be observed in Figure 4. They found that the best fluorescence enhancement occurs at the distance of 8-9 nm with EFs of ~9 for bovine serum albumin and ~6-7 for rabbit and goat IgG. With this series of articles, the group of Dr. Lakowicz successfully presented the potential of non-noble substrate for surface-enhanced spectroscopy and highlighted the ideal fabrication parameters for further studies. Overall, it is evident that the SEF research area is quite popular and has great potential in point-of-care testing and in biosensing as a whole.

1.3 Substrates and applications

In the last 40 years, the main substrates of choice for the SERS and SEF were noble metals such as gold and silver, as they possess the ability to provide and sustain intense plasmon resonances in the visible-near infrared region where the wavelength range of interest for Raman measurements is located.[49] However, rare noble metal films are relatively costly substrates and they may suffer from contamination with S-containing compounds or/and corrosion (especially Ag film).[50-51] Thus, the need for more cost-efficient, sensitive, and stable substrates with wider availability. One of such potential substrates is aluminum foil, which is plasmon tunable in a relatively broad UV and visible range.[52] There were reports of the application of aluminum as an inexpensive, versatile, and sensitive substrate for Surface-enhanced Raman Spectroscopy (SERS), with excitation in the visible range.[52-55] Besides metal substrates, the use of silicon wafer as a SERS substrate is quite popular and have shown good results in several studies.[56-58] It is significantly cheaper than plasmonic metal substrates and has remarkable stability on par with biocompatibility. Furthermore, the low plasmonic properties of the Si wafer can help to analyze the relationship between nanoparticles excluding the effect from the substrate.[59] So, these aluminum and silicon substrates have great potential as a replacement for more expensive noble materials.

According to the literature review, despite the clear advantages of silicon and aluminum substrates this research area is still new and has great prospects. Thus, my thesis project will focus on the applications of silicon and aluminum-based substrates in SERS and SEF. For the application of the silicon wafer substrate, we conducted a SERS immunoassay experiment with human immunoglobulin antibodies as an analyte. As silicon has the potential to decrease non-specific adsorption of biomolecules, which is one of the main challenges in biosensing applications and our case immunoassays.[60] As for the

application of aluminum foil substrate, we performed SEF labeling of bacterial cells with quantum dots. Which, as we know of, is the first example for the SEF detection of bacteria cells labeled with the quantum dot. In this thesis, I will present and discuss the results of these experiments and compare these nontraditional substrates with widely accepted gold and silver substrates.

[The material contained in this thesis was reproduced with permission from Sultangaziev et al.[61] and Kunushpayeva et al.[62]., Elsevier]

2.0 Materials and methods

2.1 SERS Immunoassay

2.1.1 Chemicals and consumables

Commercial microscope slide coated with gold films of 100 nm thickness (99.9% purity), over Cr (thickness = 2–3 nm) layer, were purchased from EFM Co, USA. 60 nm and 50 nm diameter Gold nanoparticles (753653-25 mL) stabilized suspensions in PBS, crystalline Si wafers, human IgG (I4506), IgG from rat serum I4131-10 mg(200227), anti-human IgG antibody produced from goat (SAB3701279), Bovine Serum Albumin (BSA) A7030–10, Casein blocking buffer, Twin 20 detergent, 4-nitrobenzenethiol (4-NBT) and any other chemicals used in the assay preparation were purchased from Sigma Aldrich. Aluminum foil tape was purchased from a nearby appliances shop. Ultra-pure water was used for all steps of the assay, and it was obtained from Millipore Direct-Q®3 UV Water Purification System.

2.1.2 Substrate preparation

Substrates are 100 nm thick commercial gold film evaporated on microscope slides or monocrystalline Silicon wafers. The surfaces of all substrates (average size 13 x 13 mm, cut with a glasscutter) were covered with pieces of parafilm, where holes of ~ 5 mm diameter were punched in with a hole puncher. To ensure adhesion between a parafilm and a substrate, the substrates with pieces of parafilm above were heated on a hotplate at 70-80 °C for 30-60 seconds, making parafilm partially melt and adhere to the surface of the substrate.

2.1.3 Substrate modification

1. 30 µL solution of 40 µg/ml anti-human IgG antibodies dissolved in Phosphate Buffered Saline (PBS, pH=7.40) was delivered on each address for 4 hours in a wet chamber

R1: First Rinsing with 0.1% Tween 20 in PBS solution, 1+1 =2 mL for each address.

2. Next, 30 µL solution of Casein Block buffer was delivered to each address, left for 3 hours in a wet chamber.

R2: Recurrent Rinsing with 0.1% Tween 20 PBS solution (PBS-T) 1+1 mL for each address

3. 30 µL solution of antigen (analyte) human IgG in PBS solution delivered on the surface of each address and left for 4 hours in a wet chamber.

R3: Recurrent Rinsing with PBS-T solution 1+1 mL for each address

4. 30 µL solution/suspension of ERLs delivered on the surface of each address and left for 8 hours in a wet chamber.

R4: Final Rinsing with PBS-T solution 1+1 mL for each address

Sample drying → Ready for measurements.

2.1.4 Preparation of ERLs (Extrinsic Raman Labels)

1. Add 10 µL of 1 mM solution of 4-NBT in acetonitrile and 50 µL of 50mM borate (pH=8.4) to 1.00 mL of 60 nm diameter suspension of gold nanoparticles in PBS in each of several micro-centrifuge tubes and shake it for 2 h

2. Centrifuge the tubes with the suspension at 2500 g for 5 minutes; remove supernatant (~0.95-0.95 mL) without disturbing gold nanoparticle at the bottom of each tube.

3. Add 1.00 mL of 2mM Borate Buffer + 140 µL of 250 µg/mL solution of capture antibody (anti-human IgG) and shake for 6 hours.

4. Add a solution of BSA (120 µL of 10% Bovine Serum Albumin) to the tube and continue to shake the tube for another 5 hours.

5. Centrifuge the tubes for 8 min at 2500 g, remove supernatant and add 1 mL of 1% BSA solution in 2mM borate buffer.

6. Repeat the previous step (2nd cycle)

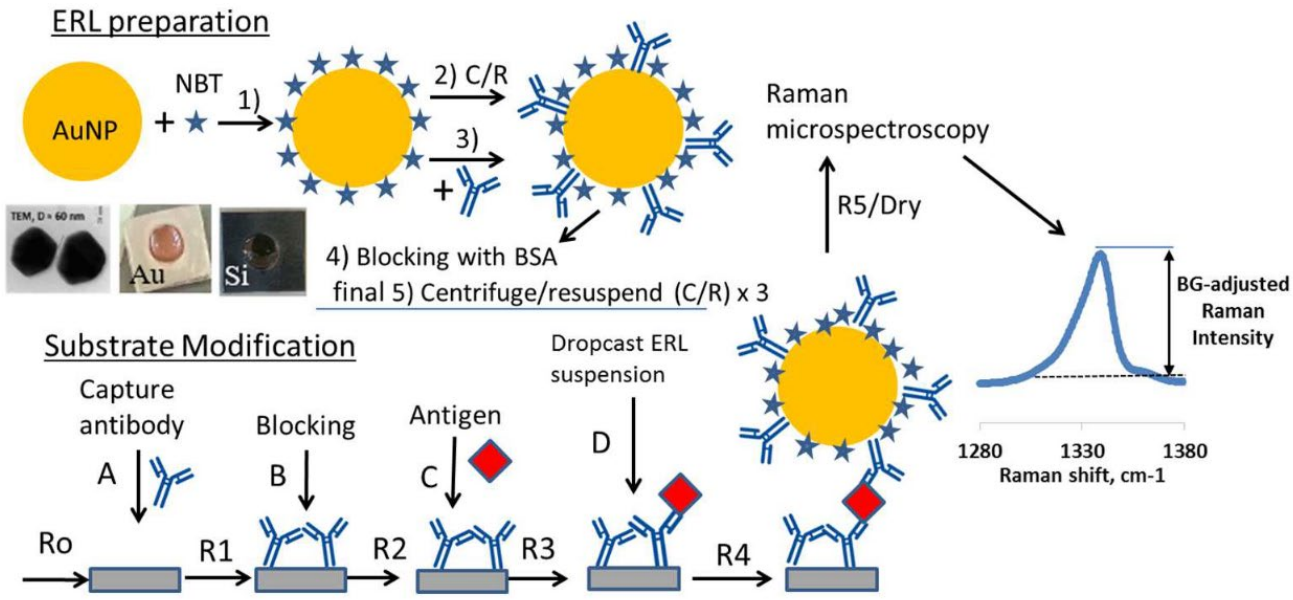

Figure 5. Immunoassay procedure. On the right inset there are TEM image of AuNPs and substrate images after ERL dropcasting.

7. Repeat the previous step but finally add 300 mL of 1% BSA solution in 2mM borate buffer and 30 μL of 10% solution of NaCl to adjust ionic strength of the suspension close to the one of human blood.

8. Combine ERLs from several 4 tubes into one tube and filtrate the suspension through a 0.2 μm pore diameter sterile syringe filter (4 mm) from Corning.

8. Apply ERL suspension to the substrate for 8 hours = Step 4 of Substrate preparation

2.1.4 Instrumentation and Measurement

Raman measurement. Confocal Raman spectrometer (LabRAM Horiba) with 785 nm laser diode and 633 nm Helium-Neon laser, along with a thermoelectrically cooled CCD detector, was used to measure Raman emission intensity in the range 1200–1700 cm−1. The instrument setup: laser power at a sample – approximately 5 mW for 633 nm, and around 10 mW for 785 nm, the objective –×10, grating - 600 g/mm, map size – 10 × 10 data points, step – 200 μm, acquisition time – 2 s, hole – 300 nm, and accumulation – 1. 5 maps are collected from each sample before averaging.

TEM measurement. TEM image of 60 nm gold nanoparticle is taken using a JEOL JEM-2100 transmission electron microscope.

AFM measurement. Smart SPM 1000 Scanning Probe Microscope system from AIST-NT was used to perform AFM measurements. The setting for AFM: cantilever (model – AppNano ACTA-50, material – Si, N-type, 0.01–0.025 Ω/cm, the radius of the tip – r < 10 nm, k=37 N/m), rate – 0.8-0.9 Hz, map resolution – 1000 × 1000 pixels, and map sizes were 6 × 6 μm.

2.1.4 Data processing and Calculations

Background corrected Raman intensities (for N-O stretching vibration in 4-NBT molecule) were calculated, with the peak maximum in the range 1320–1360 cm1 and two peak baseline ranges, 1280–1290 cm1 and 1370–1380 cm1. We calculated it by subtracting the average background (BG) (also known as the average baseline) from the maximum Raman intensity value for of spectrum. For each measurement day, all BG corrected spectra were averaged for each map and sample. We measured the assay with a 633 nm laser excitation about 2–4 days after it was completed. These are known as Week A or Week 1 data. We had to wait about a year for a new 785 nm laser to be installed. The samples were then measured with 785 and 633 nm excitation in three weeks after a year of storage: week B, week C, and week D. (for 785 nm only). To calculate blank adjusted Raman Intensity for each map, we subtracted the average blank signal (BGcorrected) from the average BG corrected signal for each case each week and sample. The LOD was calculated as an analyte concentration at three standard deviations of the blank from the plot of blank adjusted signal vs analyte concentration, using the formula shown below.

$$LOD = 10^{\left(\frac{3*STDEV-b}{a}\right)} \quad (8)$$

Where STDEV is the standard deviation in the blank signal measured on three different days, and a and b are the slope and intercept of the linear calibration plot, respectively.

Because the immunoassay response could be S-shaped, we calculated LOD using 4 parameters logistic regression analysis, a method commonly used in bioassays such as ELISA. [63] The minimum detectable concentration is reported for both types of regression analysis as the lowest measured concentration with a signal greater than three standard deviations above the blank signal, and the minimum quantifiable concentration is reported

as the lowest measured concentration with a signal greater than ten standard deviations above the blank signal.

2.2 Bacteria labeling with quantum dots for SEF spectroscopy

2.2.1 Chemicals and consumables

CdSeS/ZnS alloyed QDs (diameter 6 nm, λ emission = 665 nm), CdTe core-type QDs (diameter 3.47 nm, λ em = 610 nm), were purchased from Sigma-Aldrich. Gold, silver, and aluminum films, 100 nm thickness, on microscope glass slides were purchased from EFM Corporation, aluminum foil was purchased at a local supermarket and it was attached to microscope glass slides with double-sided adhesive tape.

2.2.2 Methodology

E. coli bacteria (DH5α) were grown aerobically overnight on a solid sterilized Luria-Bertani agar medium at temperature 37 °C. After that, the bacterial colony was added to 10 mL of Lysogeny broth, where it was cultivated for 1.5 h at 37 °C (OD600 ~ 0.1). Meanwhile, 10 mM phosphate-buffered saline (pH = 7.4) was prepared in ultra-pure water, and then it was sterilized. 0.5 mL of bacteria suspension was centrifuged at 6000g for 15 min. The pellet was resuspended in 1 mL of PBS solution, which was already used as a medium for modification of E. coli with QDs as reported in Zhu et al. publication.[64] This step was repeated two times, and after that, the bacteria culture was reconstituted in the following mixtures (1 mL each): CdSeS/ZnS QDs in PBS (1:50 and 1:25), CdTe QDs in PBS (1:50 and 1:25). The mixtures of QDs and bacteria were stirred at 100 rpm for 17 h at 37 °C. After constant stirring, the mixtures were centrifuged at 6000g for 15 min. Two more centrifugations+ resuspension cycles were done at the same rate for 10 min each. After the first two centrifugations, the pellets were resuspended in 1 mL of PBS but

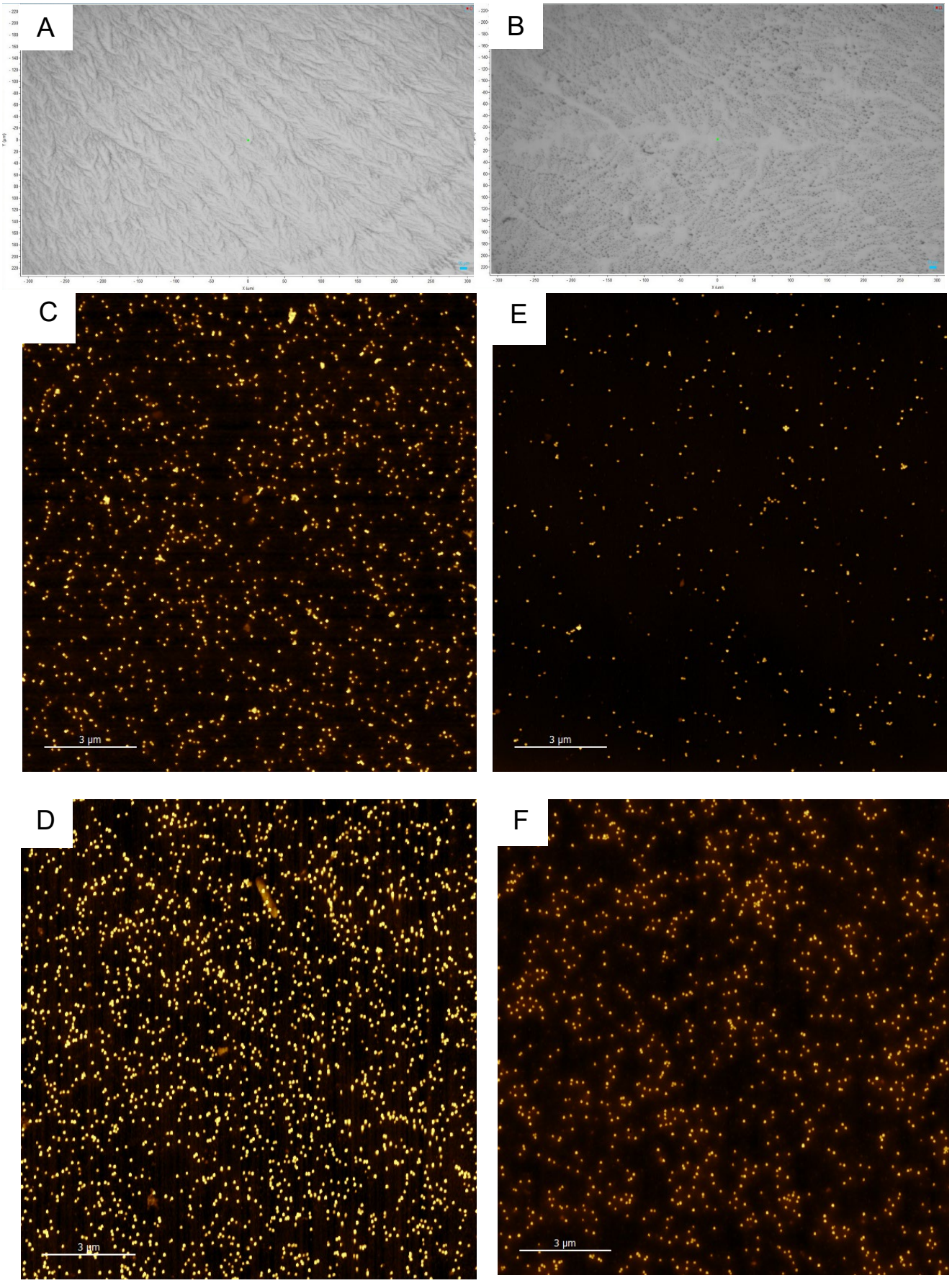

Figure 6. (A-B) x10 Optical images of Au and Si surfaces; scale – 10 µm. (C-D) AFM maps of Au, 0.3 and 1 nM; scale - 3 µm. (E-F) AFM maps of Si, 0.3 and 1 nM; scale - 3 µm.

after the third centrifugation, 400 μL of PBS was used. 10 μL of the bacteria/QDs suspension were drop-casted on the surfaces of Au film, Al film, Ag film, Al foil, and glass substrates.

2.2.3 Antimicrobial testing of Quantum dots

A standard zone of inhibition assay was conducted. Briefly, the bottom Muller-Hinton agar (MHA) with a composition of 2 g/L beef infusion solids, 17.5 g/L casein hydrolase, 17 g/L of agar, 1.5 g/L starch (BCBN0799V, Fluka) was poured on the agar plate. Bacteria were grown in a liquid broth overnight (Nutrient Broth from Titan Media containing 5g/L peptic digest animal tissue, 5 g/L NaCl, 1.5 g/L beef extract, 1.5 g/L yeast extract, pH 7.4). The next day, the bacteria were resuspended in a fresh medium and grown until OD reached 0.8. 800 μL of the cells were mixed with 80 mL of melted top MHA (3g/L beef extract, 17.5 g/L casein enzymatic hydrolysate, 8.5 g/L of agar, Titan Biotech., 1512) and poured over the bottom agar. After the top agar solidified, 3μL of the test compound was applied. The plates were incubated at 37ºC in the incubator overnight. The next day, the diameter of the zone of inhibition was measured. Antimicrobial activity was tested on Escherichia coli Dh5α cells. Penicillin at 50 mg/mL was used as a positive control. DI water and Phosphate-buffered saline (PBS) was used as a negative control.

2.2.4 Instrumentation and measurements

Fluorescence measurement. The fluorescence measurements were performed using a confocal HORIBA Labram Raman microscope with excitation wavelengths 633 nm and objective x100 for imaging of single cells. The measurement time of 1 s and the neutral density filter 1% were used for measurements with both lasers, which resulted in laser power at the sample of 0.13 mW and 0.05 mW respectively. The power was selected in order to minimize the maxing out of the detector (signal above 65,000 cps), which were

frequent for cells labeled with CdSeS/ZnS QDs on gold and Al foil (up to 30% of spectra) at a higher laser power of 2.5%. The signals are averaged from 10 to 20 spectra of QD labeled single cells, 6–8 spectra of control cells, and 6 spectra of the background taken with ×100 objective.

SEF enhancement factor and contrast calculation. MEF enhancement factors are calculated as the ratio of fluorescent signal (maximum average spectra intensity) on metal film to the same kind of signal on the glass substrate. Contrast is calculated as a ratio of signal from QD labeled bacteria cell to signal from unlabeled (control) cell on the same substrate and same spectra acquisition parameters.

SEM measurement. SEM images were obtained by Carl Zeiss Crossbeam 540.

Energy Dispersive X-ray spectroscopy (EDS). Spectra obtained on the same SEM microscope with X-Max 150 detector from Oxford Instruments.

AFM measurement. Smart SPM 1000 Scanning Probe Microscope system from AIST-NT was used to perform AFM measurements in tapping mode, using cantilevers: NSG10DLC (from Nanotunning.com) and NSG30 (from Tipsnano.com), frequency 240–440 kHz.

3.0 Results and Discussion

3.1 SERS Immunoassay

The main results of the experiment as the Raman spectra and calibration plots can be observed in Figures 7 and 8. For both types of SERS-active substrates, the averaged SERS spectra (A, C) on these figures show a strong pattern of increasing Raman intensity with increasing antigen concentration. Analyte signals on the gold substrate are about one order of magnitude higher than on the silicon substrate. When we use data averages from all three weeks of measurements, we can calculate the overall trend for five data points (30 to 4000 pM) as a linear logarithmic trend for two substrates and both lasers (633 nm and 785 nm), with R^2 values marginally higher on Si (0.97 and 0.98) than R^2 values on gold (0.95 and 0.97). However, since the calibration pattern for a biomarker SERS assay can be close to that of ELISA assays, it can be interpreted as a curve, which can be approximated using 4-parameter logistic regression analysis.[65] As a result, we calculated LODs using two methods: the first ("conservative") from the linear section of the calibration plot (10, 100, 300, 1000, 4000 pM) and the second using a four-parameter

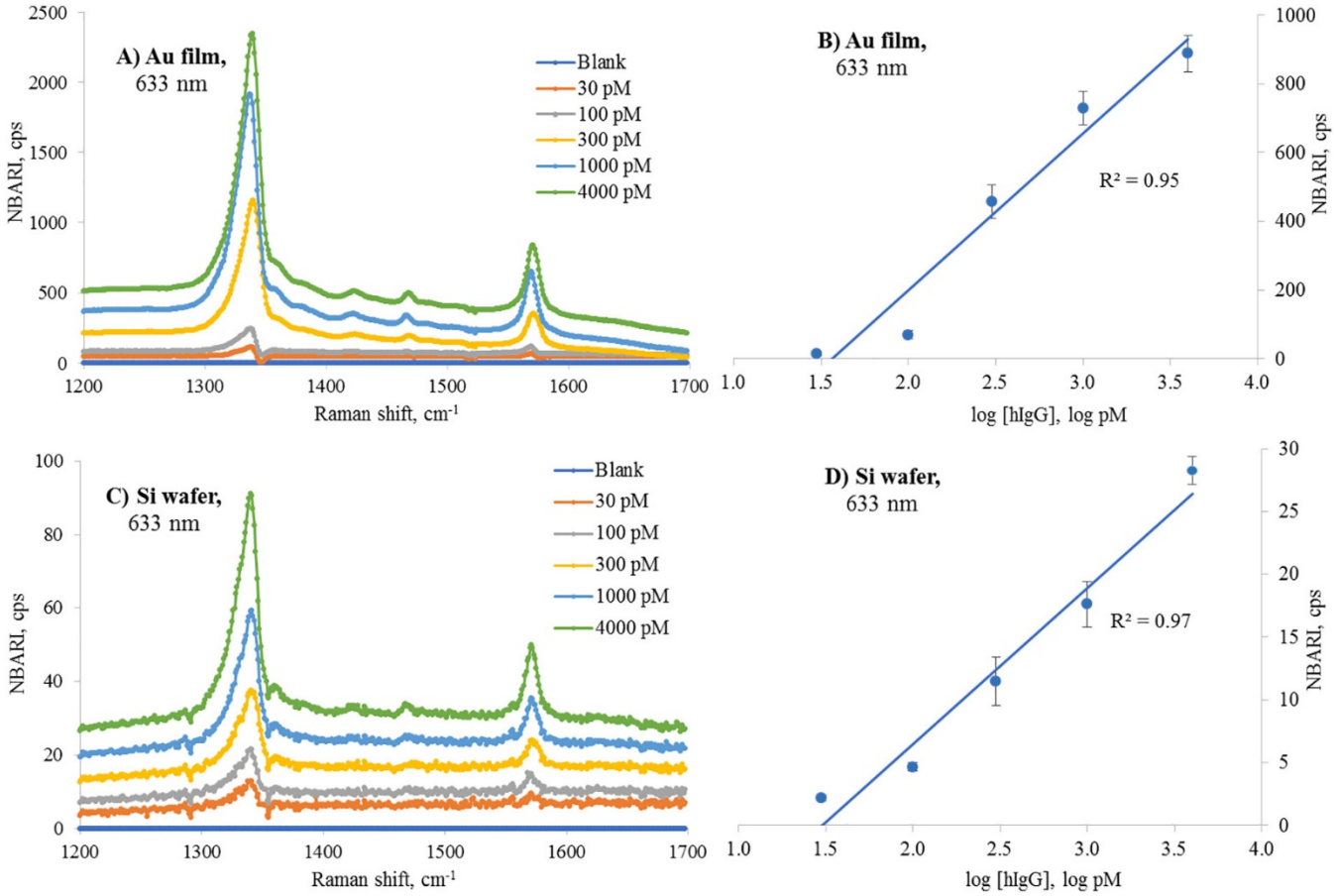

Figure 7. SERS spectra (A, C) and calibration plots (B, D) for the sandwich immunoassay of hIgG on gold film and Si substrates obtained with a 633 nm laser. NBARI is normalized blank adjusted Raman intensity, which was averaged from three sets of measurements performed on different weeks.

logistic model (see Tables 1 and 2 and Figure 9 for details). When we use "conservative" linear logarithmic calibration, the signal and slope usually decrease from week A to week B and C, and LODs generally increase. After the first measurement, the LOD for both gold and silicon assays got a little worse, as seen in Table 1. For the gold assay, it went from 34 to 39, 40 pM, and for silicon assay, it went from 25 to 38, 37 pM. For both gold and silicon assays, the linearity R^2 for calibration plots dropped from 0.97 to 0.93–0.95 as samples were re-measured. The origin of this trend is quite straightforward, as the samples lose their plasmonic properties with time due to thiol desorption and partial sample bleaching during measurements with laser light. Nevertheless, results showed that the calibration plot remained more or less unchanged even after a year between measurements of sample batches from weeks A and weeks B and C with a 633 nm laser, indicating that the samples are somewhat stable and capable of multiple re-measurements after a few months. Although, the measurements within just one week after assay completion produced the best results. Nonetheless, the durability of samples prepared by this method might be used as an advantage in the detection of so-called doping or prohibited substances in sport or forensic analysis.

LOD values measured using a "conservative" method for gold and silicon assays using a 785 nm excitation laser are comparable to those obtained using a 633 nm excitation laser. In particular, the LODs were 33 pM on gold and 28 pM on silicon, but the logarithmic pattern R^2 on gold was not as successful as R^2 on silicon (0.96 and 0.98, respectively). When we switched from 633 nm laser excitation to 785 nm laser excitation, the scale (SERS signal) and slope on calibration plots decreased by around a factor of two

for both gold and silicon. This is to be anticipated, given that the LSPR resonance of gold nanoparticles (max in suspension 540 nm) on both gold film and silicon should be closer to 633 nm than the excitation wavelength of 785 nm. Thus, for the measurements of

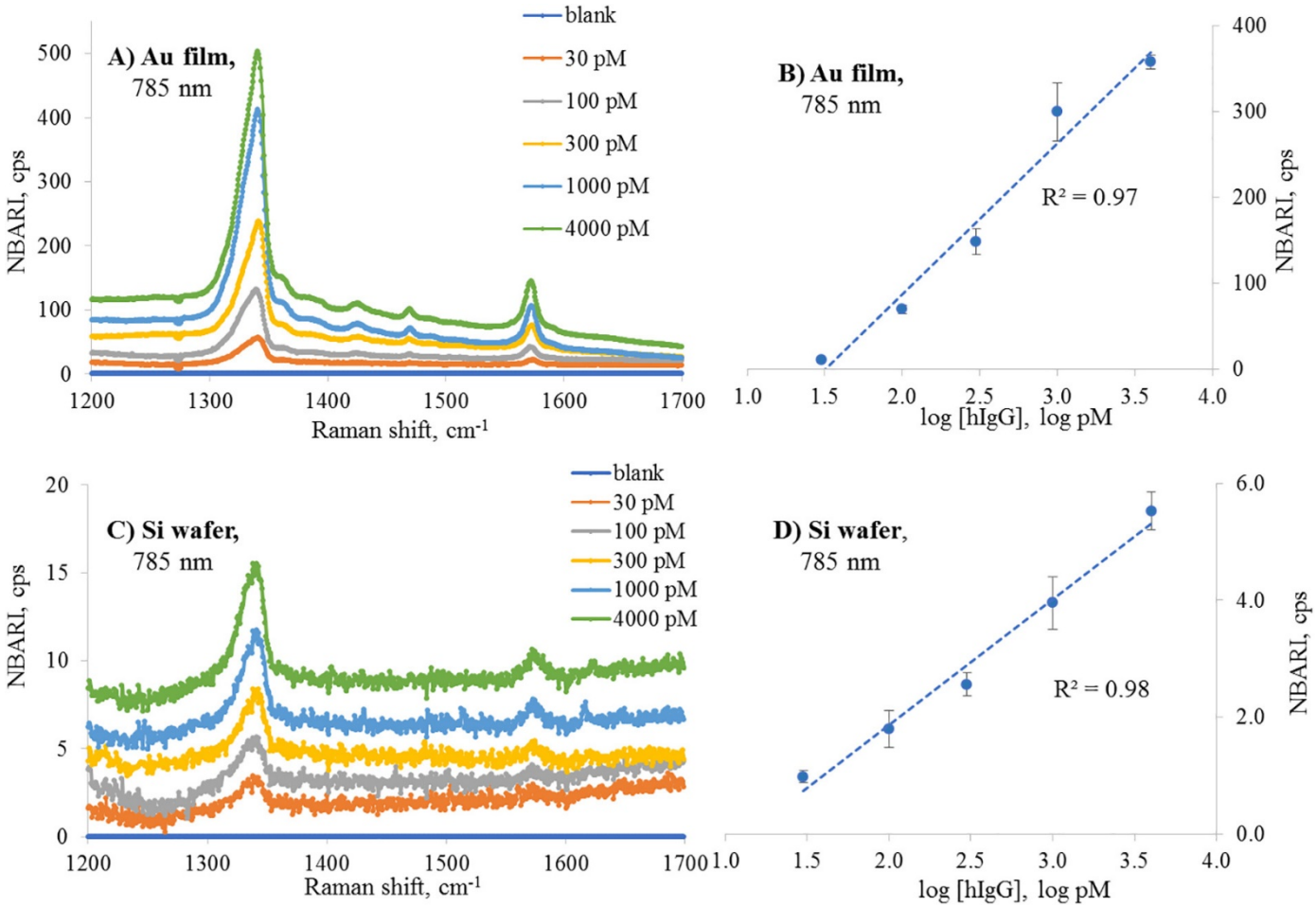

Figure 8. SERS spectra (A, C) and calibration plots (B, D) for the sandwich immunoassay of hIgG on gold film and Si substrates obtained with a 785 nm laser. NBARI is normalized blank adjusted Raman intensity, which was averaged from three sets of measurements performed on different weeks.

sandwich SERS immunoassays on both gold film and silicon substrates, 785 nm lasers can be used just as well as 633 nm lasers for any practical applications.

Moreover, it is worth noting that the slope of signal vs log [hIgG] on the calibration plot for gold, is much higher than the same kind of slope for the assay on silicon. This difference would improve the LOD according to the formula mentioned in materials and methods, but there is a strong opposite effect from a far lower standard deviation of the blank on silicon relative to the standard deviation of the blank on gold (e. g 0.22 cps vs 3.01 cps respectively for week A, 633 nm measurements). Even relative standard deviations for the signal on silicon are roughly two times lower than corresponding relative standard deviations for the signal on gold. For example, for a concentration of 30pM of hIgG, the average RSDs for two lasers are 12.1 percent on gold and 5.5 percent on silicon. This observation shows that the decrease in signal variability can have the same magnitude of impact on the LOD as signal intensity.

However, by using the four logistic parameter model, the LOD for silicone is significantly lower than LOD for gold as shown in Figure 9: 3 pM and 28 pM respectively. Thus, we can confirm that the silicone substrates have a comparable level of performance in terms of the lowest detectable concentration as gold substrates for this type of SERS immunoassay. Also, it is important to choose the right model for the calculations of analytical parameters, as they can produce significantly different results.

Figure 10 shows the representative AFM maps for samples with increasing hIgG concentrations: blank samples (0), 300, and 1000 pM. The number of nanoparticles per zone is increasing on both substrates, as the concentration of binding antibodies is increasing. Table 3 includes numerical data from 36 AFM maps in six samples, with data for 5060 nanoparticles (ERLs). From Table 3, we can observe that the number of ERL per

Table 1. Limit of Detection Calculations for SERS Data for 633 nm excitation: human IgG assay on Gold film and on Silicon wafer

Substrate	Data set	St. Dev	Slope	Intercept	R^2	LOD, pM
Gold film	Week A	3.01	371.8	-562.1	0.97	**34**
	Week B	3.22	488.9	-770.7	0.93	**39**
	Week C	1.44	509.1	-812.5	0.95	**40**
Silicon wafer	Week A	0.22	12.0	-16.2	0.97	**25**
	Week B	0.13	12.3	-19.1	0.94	**38**
	Week C	0.14	13.1	-20.2	0.94	**37**

Table 2. Limit of Detection Calculations for SERS Data for 785 nm excitation: human IgG assay on Gold film and on Silicon wafer

Substrate	Data set	St. Dev	Slope	Intercept	R^2	LOD, pM
Gold film	Week B	1.78	179.3	-265.9	0.97	**33**
	Week C	0.88	172.4	-263.2	0.93	**35**
	Week D	6.67	113.0	-166.0	0.95	**44**
Silicon wafer	Week B	0.29	2.3	-2.5	0.97	**28**
	Week C	0.11	2.0	-2.5	0.94	**23**
	Week D	0.12	1.6	-1.8	0.94	**23**

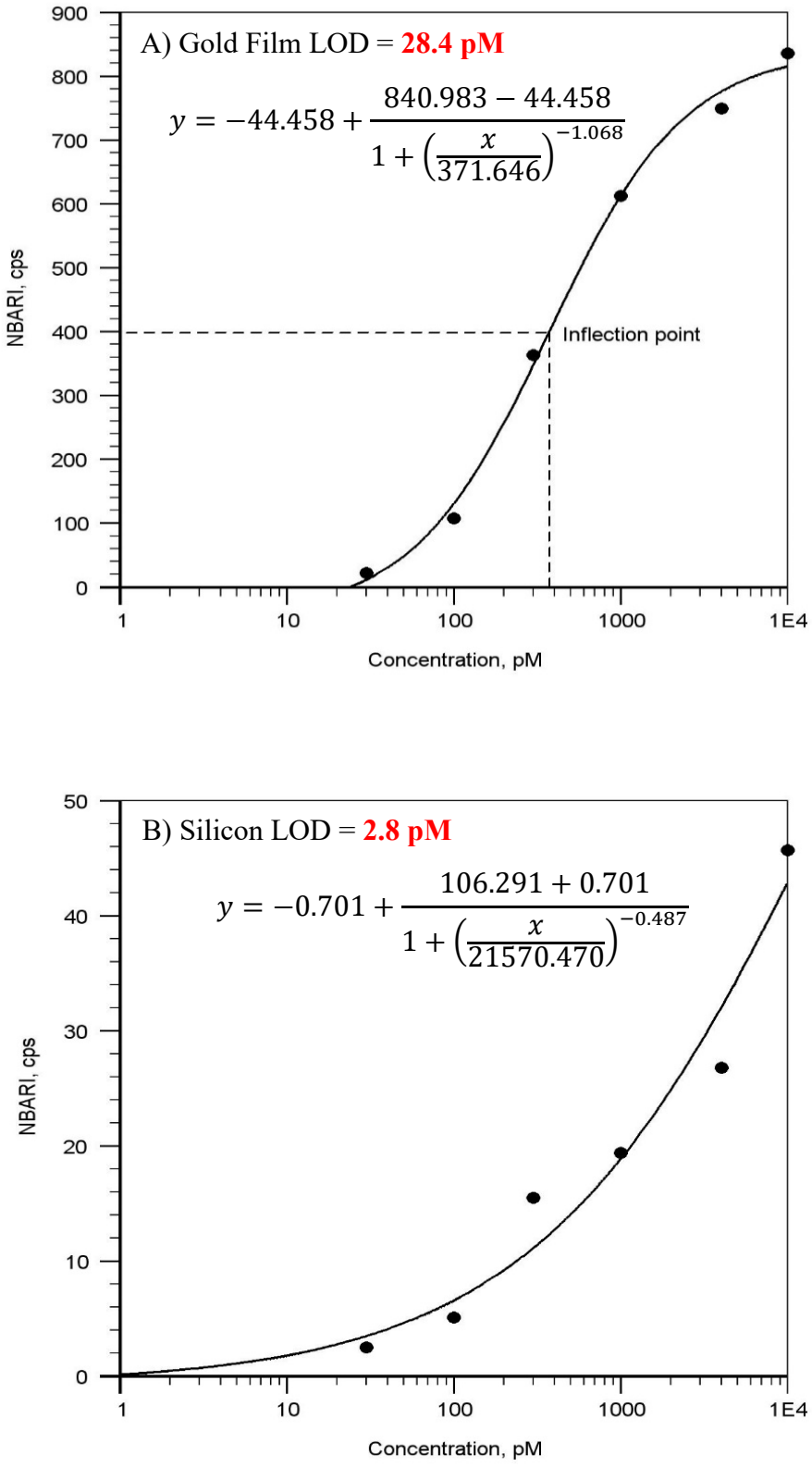

Figure 9. Calibration curves obtained by 4 parameters logistic non-linear regression analysis for Gold and Silicon substrates on the first week (week A).

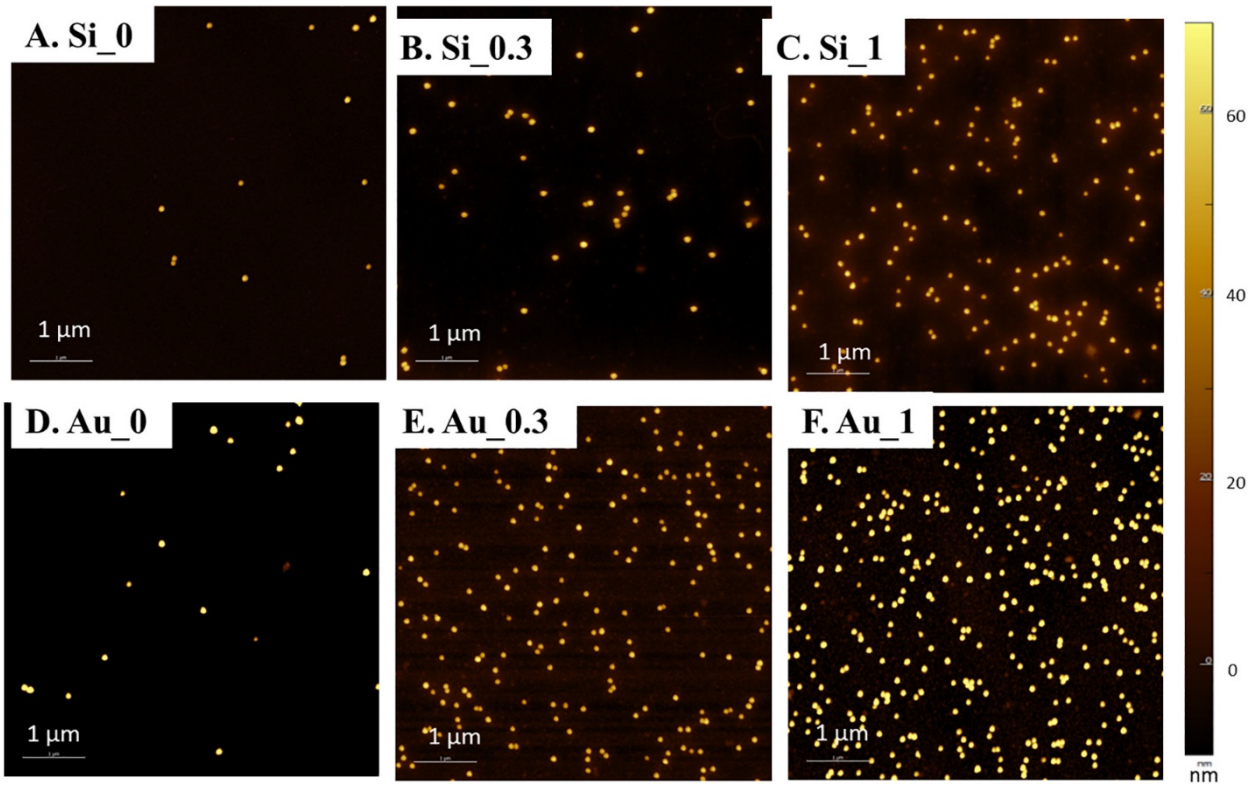

Figure 10. Representative AFM maps of increasing hIgG concentration: 0 (blank), 0.3 nM, 1 nM for A, B, C – Si, and D, E, F – gold film substrates.

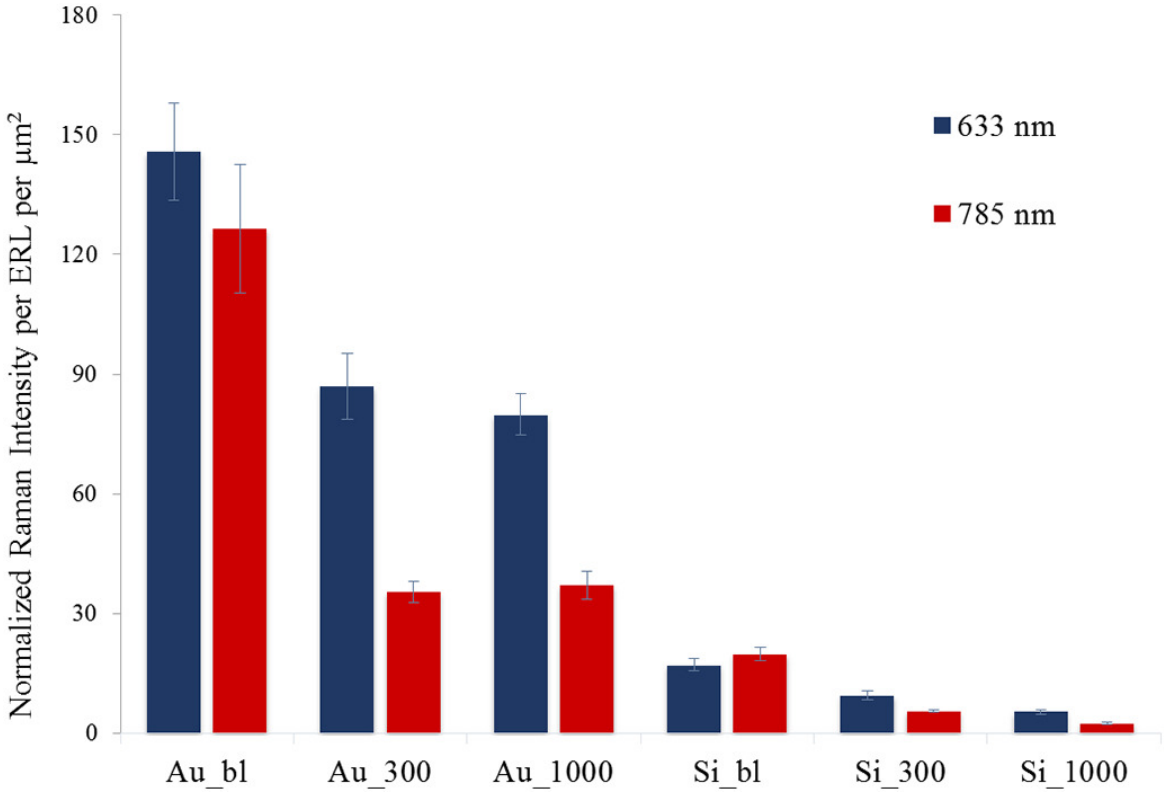

Figure 11. Normalized Raman intensity per (ERL per Area, µm2) for 633 nm and 785 nm lasers on Si and gold film substrates at various concentrations of human IgG from blank to 300 pM and 1000pM.

Table 3. Correlation of Raman and AFM Data and Calculation of Average Signal per one nanoparticle

Laser λ, nm	Sample: Substrate, hIgG concentration	Norm. Raman Intensity	Ratio Signal/(# ERL/Area, μm^2)	Number ERL/Area, NPs/μm^2	Number ERLs counted from AFM
633	Au, blank	79.67	**145.8**	0.55	118
	Au, 300 pM	537.48	**87.0**	6.33	1368
	Au, 1000 pM	808.99	**79.9**	10.13	2188
	Si, blank	6.42	**17.1**	0.38	81
	Si, 300 pM	17.95	**9.5**	1.56	336
	Si, 1000 pM	24.1	**5.4**	4.49	969
785	Au, blank	69.13	**126.5**	0.55	118
	Au, 300 pM	224.54	**35.5**	6.33	1368
	Au, 1000 pM	376.16	**37.1**	10.13	2188
	Si, blank	7.43	**19.8**	0.38	81
	Si, 300 pM	8.58	**5.5**	1.56	336
	Si, 1000 pM	11.45	**2.6**	4.49	969

unit of the area increases from 0.55 to 6.5 to 10.1 ERL/μm^2 on gold. On silicon, it increases from 0.38 to 1.6 to 4.5 ERL/μm^2. This can be explained by better binding of ERLs to the gold surface due to the specific interaction between antibodies and gold. Overall, the correlation between the surface concentration of ERLs (ERLs/μm^2) and the measured background adjusted Raman Intensity is quite high for both substrates, with an average (of 633 and 785 nm excitation) R^2 equal to 0.98. This means the signal is mainly produced from the hotspots generated by ERLs.

We also calculated the ratio of Raman intensity to Number ERL/Area (ERLs/μm2) for all six samples with both lasers, which can be observed in a bar graph in Figure 11 and Table 3. This figure shows that silicon wafer has one order of magnitude lower signal per nanoparticle ratio than gold film. Moreover, from Table 3, we can calculate that on average, the ratio of Raman signal per ERL on gold to this parameter on silicon, for the same antigen concentration, is about 11 for 633 nm excitation and about 9 for 785 nm excitation. This

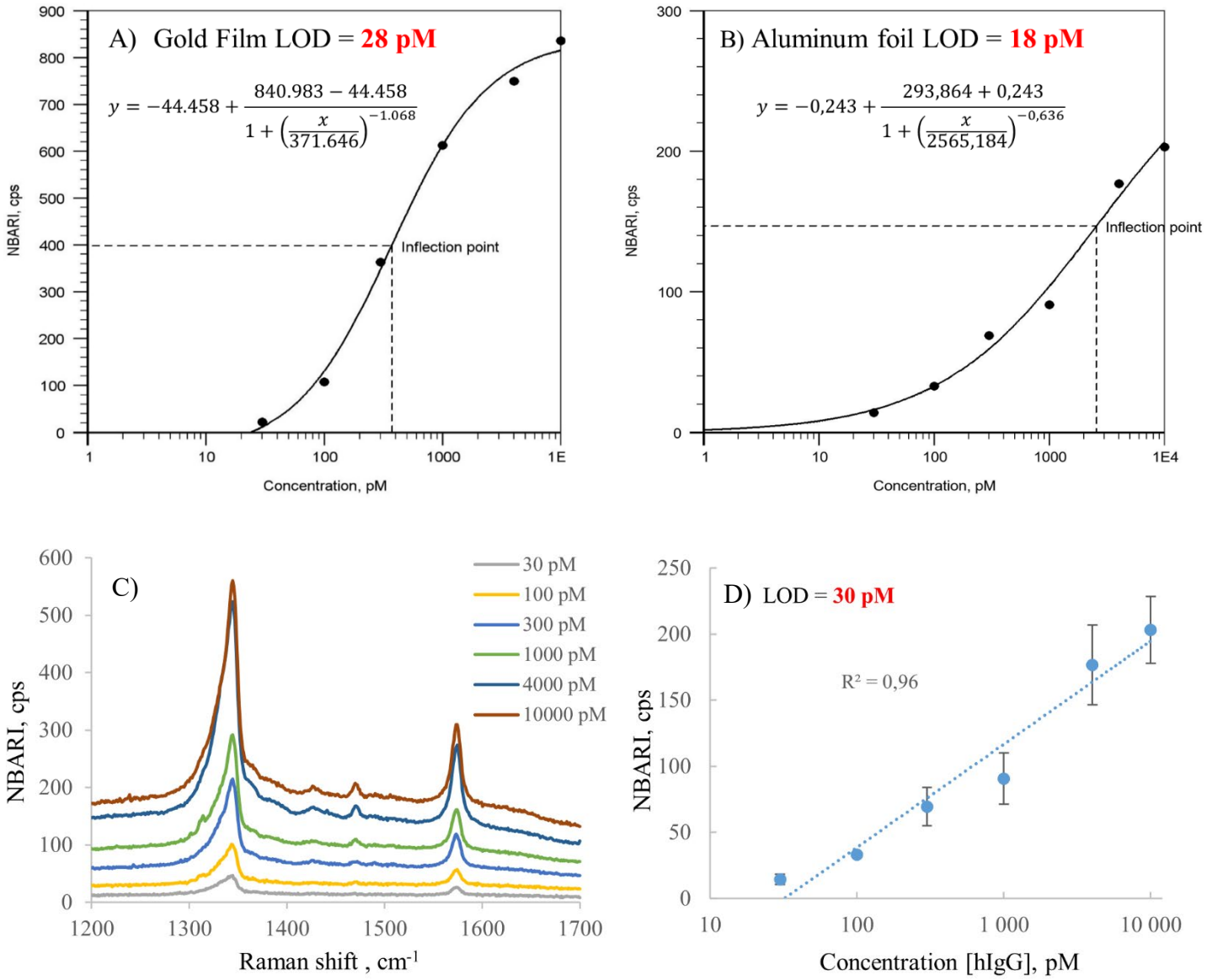

Figure 12. A) and B) Calibration curves obtained by 4 parameter logistic non-linear regression analysis for Gold and Aluminum substrates. SERS spectra (C) and calibration plot (D) for the sandwich immunoassay of hIgG on Aluminum foil, obtained with a 633 nm

observation is in agreement with the ratio of SERS enhancement factor (EF) on gold to the EF on silicon, calculated from a combination of Raman and AFM maps in the publication of Sergiienko et al.[66] However, Figure 11 also shows some decrease in Raman signal per nanoparticle as the concentration of antigen increases, particularly between a blank and 0.3 nM concentration of human IgG. Fractions of single nanoparticles among all the nanoparticles counted in the assay did not change very much from sample to sample on both substrates, remaining within 70 to 80%. The average fraction of single ERLs was quite similar for silicon and gold: 77% and 76% of ERLs were singles, on silicon and gold film respectively. Thus, we may hypothesize that another factor is responsible for this decrease in signal per ERL, or an equivalent decrease in the enhancement factor when an antigen concentration increases with the number of ERLs. For example, it is possible that the LSPR coupling between substrate and gold nanoparticles is weakened upon the increase of ERL-substrate distance due to an increase in antibody number. Which consequently decreases the EF of the SERS signal from the 4-NBT molecule. Moreover, the increase in surface concentration of nanoparticles decreases the extinction cross-section of each nanoparticle and so the SERS EF. Nevertheless, these effects are not very large. well within a factor of 2 for 633 nm laser and a factor of 3 for 785 nm laser. These negative effects can be observed for the assays on both substrates. Nonetheless, the magnitude of this change is non-significant and does not have a detrimental effect on the assay performance for the concentration range between 30 and 4000 pM.

In addition, we conducted immunoassay on the surface of aluminum foil and performed a selectivity experiment using human and rat IgG antibodies with three substrates: gold film, aluminum foil, a silicon wafer. Results of the immunoassay on the aluminum foil substrate can be observed in Figure 12. Similarly to the silicon wafer and

Table 4. Selectivity of SERS immunoassay for human IgG against rat IgG on three substrates. NBARI – normalized blank-adjusted Raman intensity

Substrate	Concentration, pM	NBARI for human IgG, cps	NBARI for rat IgG, cps	The ratio between NBARI for human IgG and rat IgG
Gold film	500	1.03	0.130	12.6%
	2000	7.03	0.686	9.7%
Aluminum foil	500	2.53	0.250	9.9%
	2000	6.16	0.470	7.6%
Silicon wafer	500	1.07	0.008	0.7%
	2000	2.07	0.040	1.9%

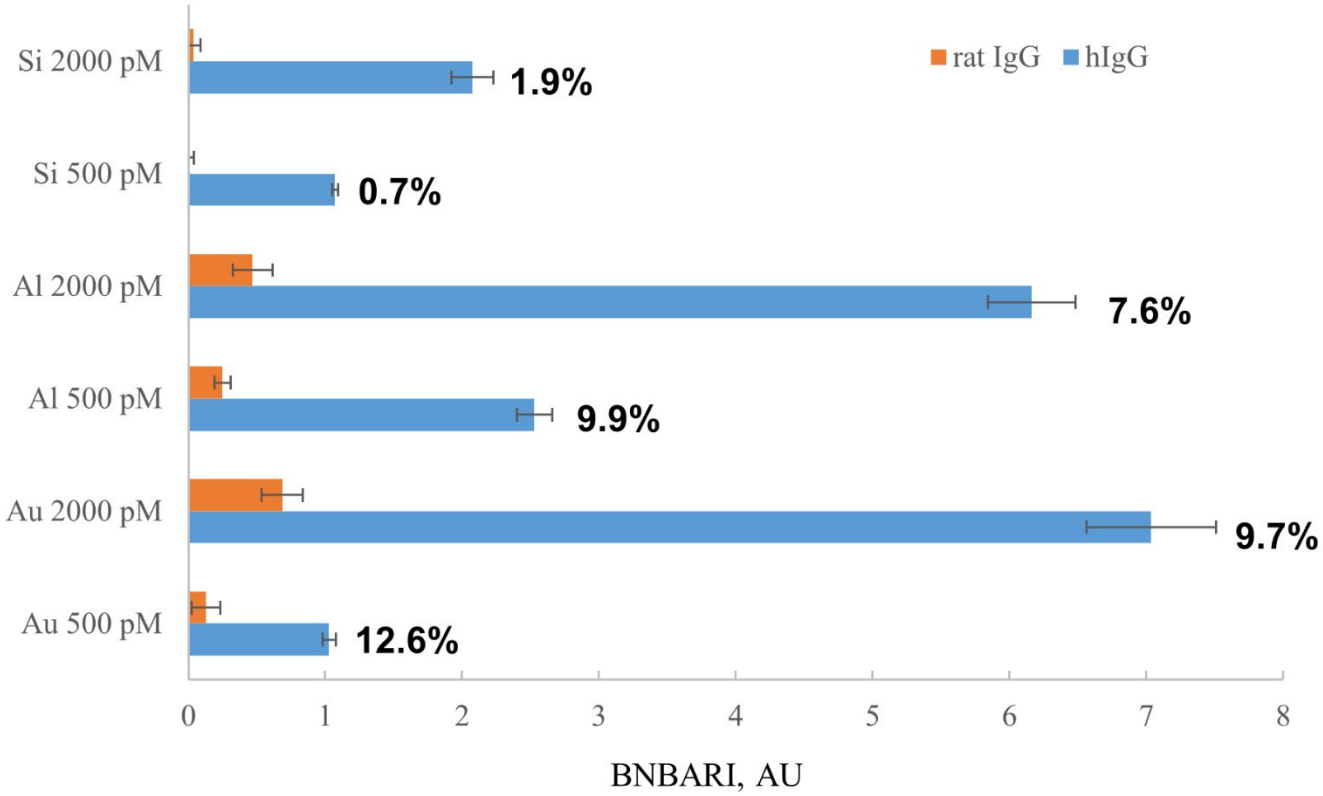

Figure 13. Selectivity bar graph. Blank Normalized Blank adjusted Raman intensity for Si wafer, Al foil and gold film at various concentrations of human IgG and rat IgG. All signals are normalized to blank signal on each substrate.

gold film the results for Al foil were analyzed by using logarithmic fitting and four-parameter logistic non-linear regression analysis. LODs found by these methods were 30 pM and 18 pM respectively. So, the sensitivity of Al foil is on par with Au film and slightly lower than Si wafer. As for the selectivity experiment results, spectra obtained from the Raman measurements of 500 and 2000 pM concentrations can be seen in Figure 14. From these spectra, we can observe that signal intensity increases from silicon wafer to aluminum foil to gold film. Data for this observation can be seen in Table 4. On the other hand, the trend of specificity is reversed with silicon wafer demonstrating significantly better ability to discern between hIgG and rat IgG. So, silicon wafer demonstrates 8-9 times better average specificity than gold film (1.3% vs. 11.2% relative non-specific signal) despite 8 times lower intensity, which is mainly due to non-specific binding of antibodies. These differences can be better observed from bar graph in Figure 13. The non-specific signal from rat IgG on aluminum foil is on average about 30% lower than the signal on gold film (8.65% vs. 11.2%).

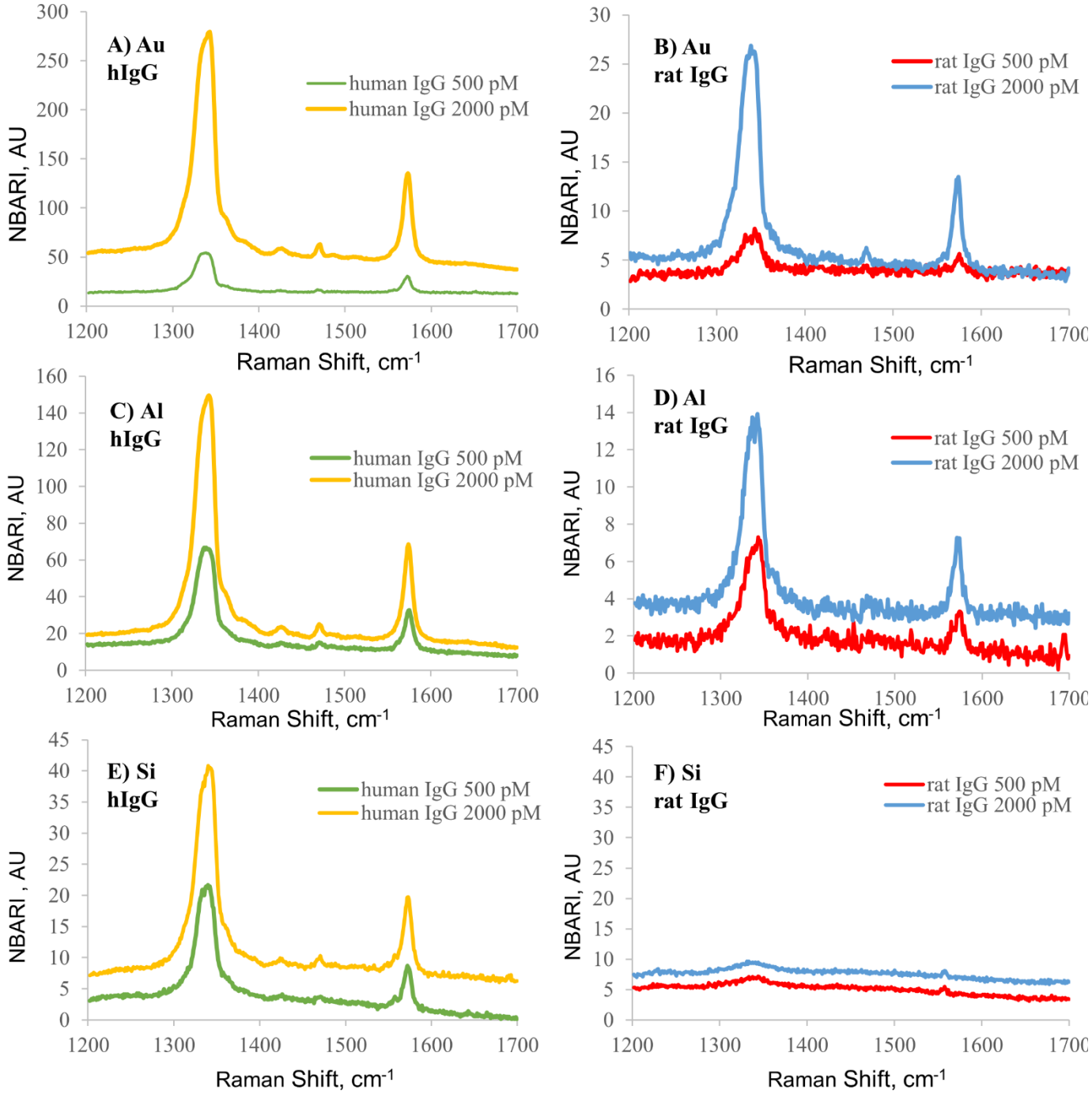

Figure 14. Raman spectra of gold film with hIgG (A), rat IgG (B); aluminum tape with hIgG (C), rat IgG (D); silicon wafer with hIgG (E), rat IgG (F). NBARI – normalized blank-adjusted Raman intensity, AU – arbitrary units.

3.2 Bacteria labeling with quantum dots for SEF

Antibacterial activity of QDs is demonstrated in Figure 15, where gray spots indicate zones of inhibition of bacterial growth. We can observe that there are no such spots for various concentrations (10, 20, 40, 100 ppm) of CdSeS/ZnS QDs (Figure 15A) with only the control spot (from penicillin) being visible on the dish. We may therefore infer that these QDs are not only non-toxic at the concentration levels used in the experiment (40 ppm) but at 100 ppm, which can yield even higher emission intensity and even higher MEF. The literature about QD toxicity backs up our findings. CdSeS/ZnS quantum dots are core-shell structured QDs, where the core is CdSeS and the shell is ZnS, which is non-toxic. According to Li et al. and Fu et al., ZnS is chemically stable and demonstrates passivating properties that prevent decomposition and oxidation of the core and consequently prevent toxic Cd^{2+} ions from releasing to the environment.[67-68] Moreover, Jaiswal et al. labeled living cells using similar kinds of CdSe/ZnS QDs and found no adverse effect on the growth

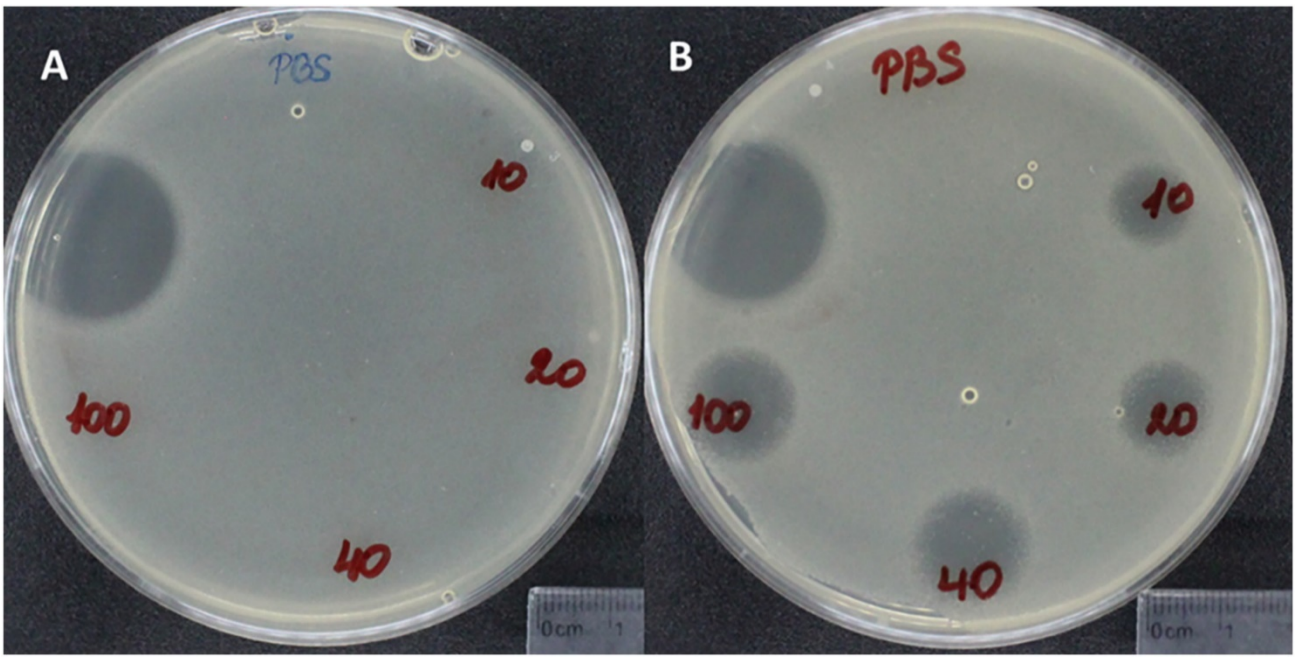

Figure 15. Images of two bacterial plates in cyto-toxicity (antimicrobial activity) experiment: A) 10, 20, 40, 100 ppm of CdSeS/ZnS QDs in PBS. B) 10,20,40, 100 ppm of CdTe CDs in PBS. Both plates have spot of PBS solution and penicillin solution (the largest spot) as controls.

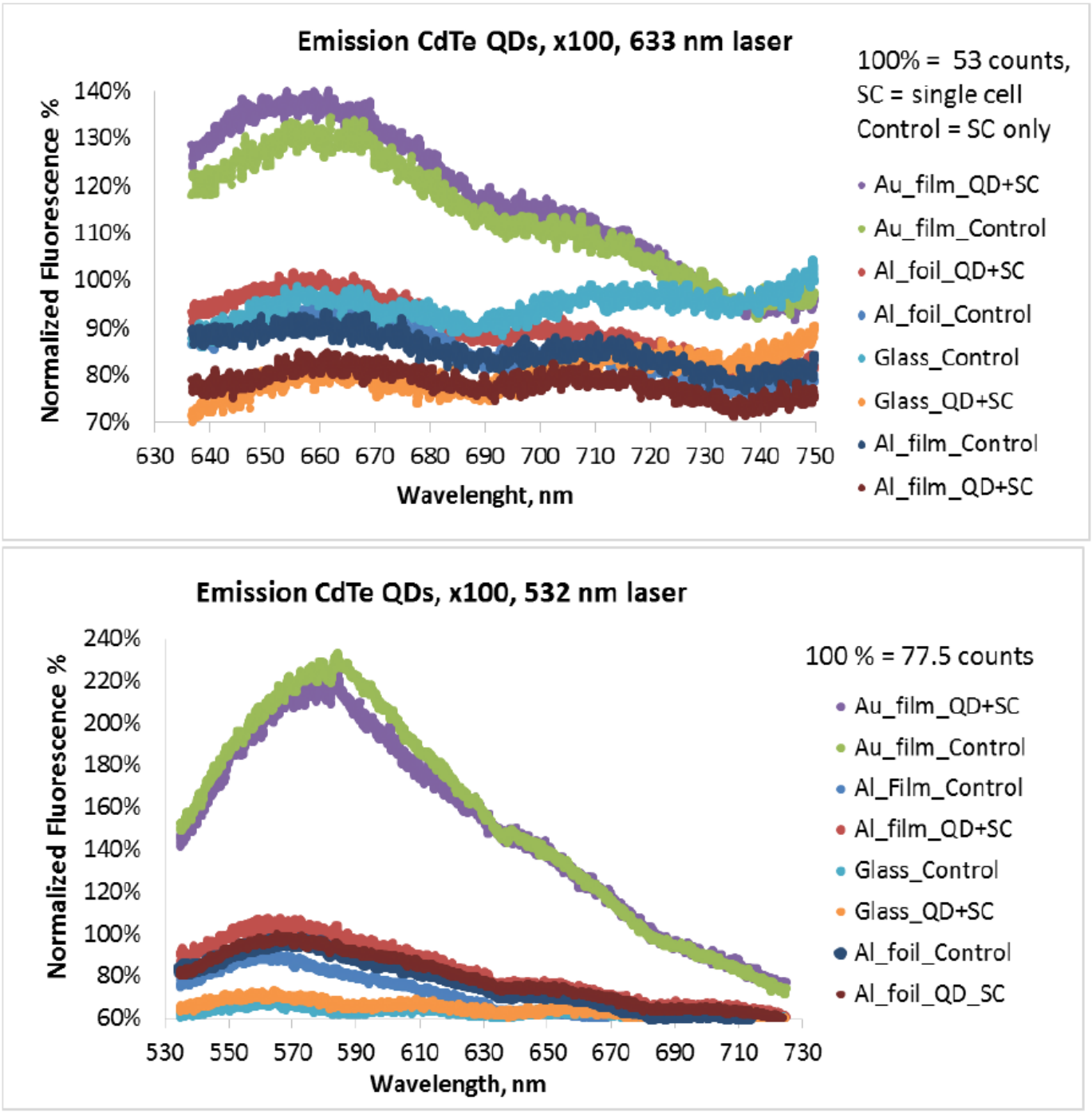

Figure 16. Averaged Normalized Fluorescence Emission spectra of CdTe QDs with single cells (QD+SC) and of control (just bacteria or SC) on various substrates, obtained with 633 nm (top) and 532 nm (bottom graph) laser excitation wavelength and x100 objective. Maximum intensity for spectrum QD+SC on Al foil is set as 100% (53 and 77.5 counts respectively).

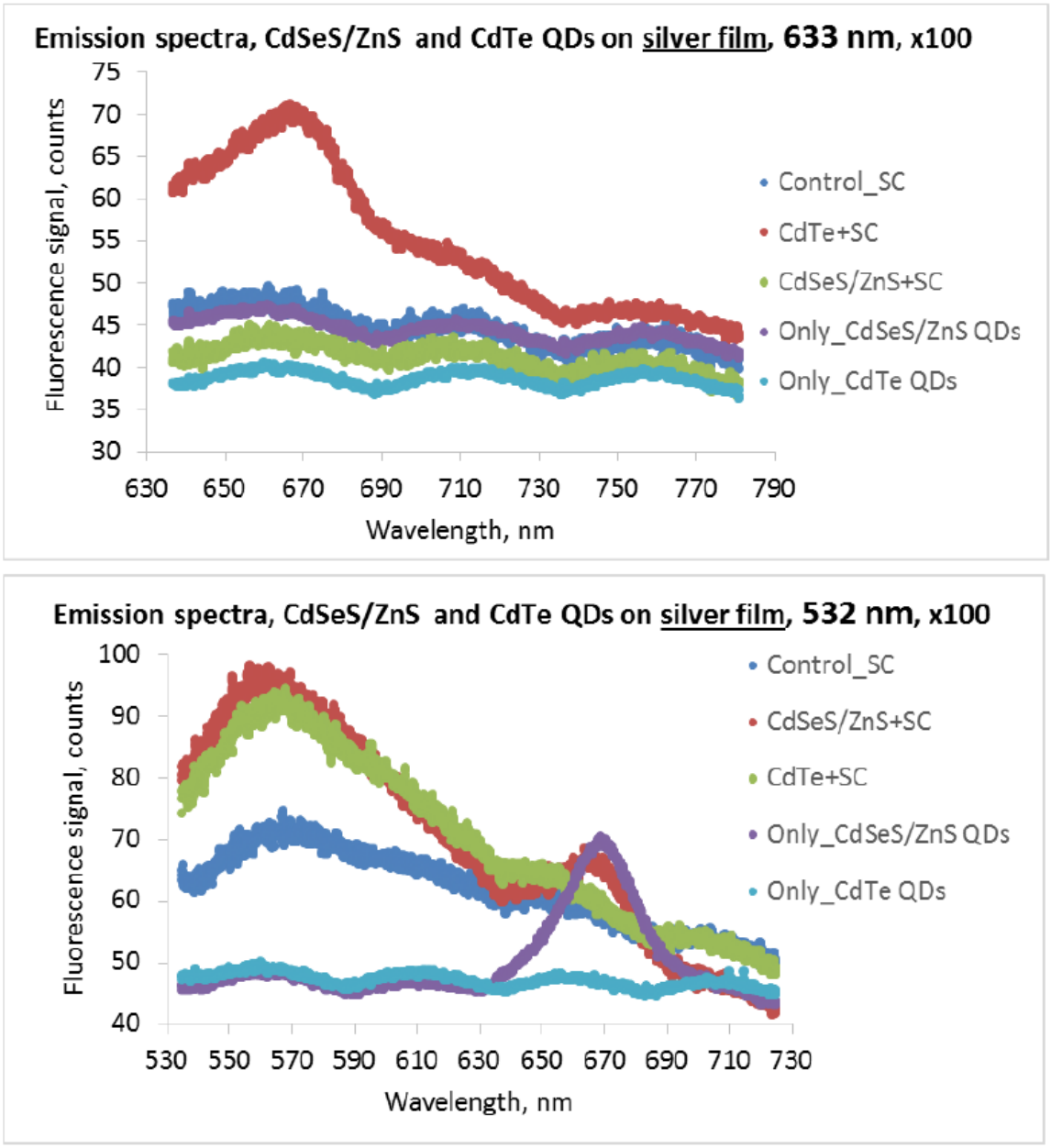

Figure 17. Averaged Fluorescence Emission spectra of CdSeS/Zn and CdTe QDs with single bacterial cells (QD+SC) and of control (just bacteria or SC) on silver film substrate, obtained with 633 nm (top) and 532 nm (bottom graph) laser excitation wavelength and x100 objective. Only_QDs are spectra of both QDs in PBS dropcasted on silver film.

and cell signaling of those cells.[69] On the other hand, CdTe QDs demonstrate cell toxicity since a clear gray spot appears on Figure 15B even for 10 ppm with larger spots for higher CdTe QD concentrations. The toxicity of those QDs is also consistent with scientific literature. As an example, Li and co-workers determined the half inhibition concentration of QDs (IC50), the growth rate constant (k), and optical density (OD) of E. coli mixed with different concentrations of CdTe QDs.[70] They found that the higher the concentrations of CdTe QDs starting from 80 nM, have a detrimental effect on both the growth rate constant k and OD of bacteria.

As shown in Figure 16, for spectra taken from signal cells (x100) with both 533 and 632 nm excitation lasers, CdTe QDs labeled bacteria do not display noticeable enhancement factors, which are ratios of signal on metal substrates to signal on glass. For example, MEF EFs for 633 nm are in the range of 1.0 to 1.6. Those QDs often lack clear contrast, which is defined as the ratio of the average signal of the QD labeled cell to the average signal of the control (unlabeled) cell. When contrast ratios from both 532 and 633

Table 5. SEF Enhancement factors and contrast factors calculated for CdSeS/ZnS QDs in bacteria single cells (x100 objective) and QDs with majority of bacteria cells aggregated, obtained with x10.

Substrate, 633 nm	QD + SC, contrast at Max peak	QD + SC, EF at Max peak	QD only, EF at Max Peak	Substrate, 532 nm	QD + SC, contrast at Max peak	QD + SC, EF at Max peak	QD only, EF at Max Peak
Al foil	356	324	45	Al foil	317	398	20
Au film	373	476	44	Au film	69	159	20
Al film	129	145	23	Al film	23.4	226	30
Ag film	1	1	0.7	Ag film	1.1	1.3	0.6
Glass	N/A	1	1.0	Glass	N/A	1.0	1.0

nm excitation were measured, the contrast was around 1.0–1.2. Overall, CdTe QDs have not shown adequate MEF (or SEF) performance for labeling bacteria cells, most likely due to their toxicity.

As can be seen in Figure 17, CdSeS/ZnS and Cd/Te QDs in single bacteria cells (x100) on silver film substrate showed no visible enhancement factors or contrast. Table 5 indicates that the maximum contrast observed for any QD at any imaging condition for the untreated silver film is 1.6, with a maximum enhancement factor of about 1.3. MEF's figure of merits (FOMs) on silver film is about two or three orders lower than the same FOMs on three other metallic substrates. As seen in Figure 17, the absolute value of the emission peak at 665–670 nm for CdSeS/ZnS QDs in single cells on silver film (or any other QD measurement done on silver) is less than 70 cps for 633 nm excitation wavelength and less than 100 cps for 532 nm excitation wavelength for CdSeS/ZnS QDs in single cells on silver film. Since silver ions' toxicity to bacterial cells has been well documented, we believe that this antimicrobial activity prohibits the use of silver film as a substrate for MEF of bacteria with QDs. [71] Also, CdSeS/ZnS QDs on all substrates demonstrate an emission peak around the same wavelength of 665–670 nm, as expected from the specification of those QDs.

The average emission spectra of a single bacteria cell labeled with CdSeS/ZnS QDs are shown in Figures 18 and 19. When excited with any (633 or 532 nm) laser, these show very high fluorescence signal on aluminum foil (here maximum is normalization factor 100 percent or 17,970 cps for 633 nm excitation and 18,103 cps for 532 nm excitation), gold film, and aluminum film, compared to the same kind of signal on glass, although the latter fluctuates near 0.3 percent of the signal on Al foil. With a 633 nm

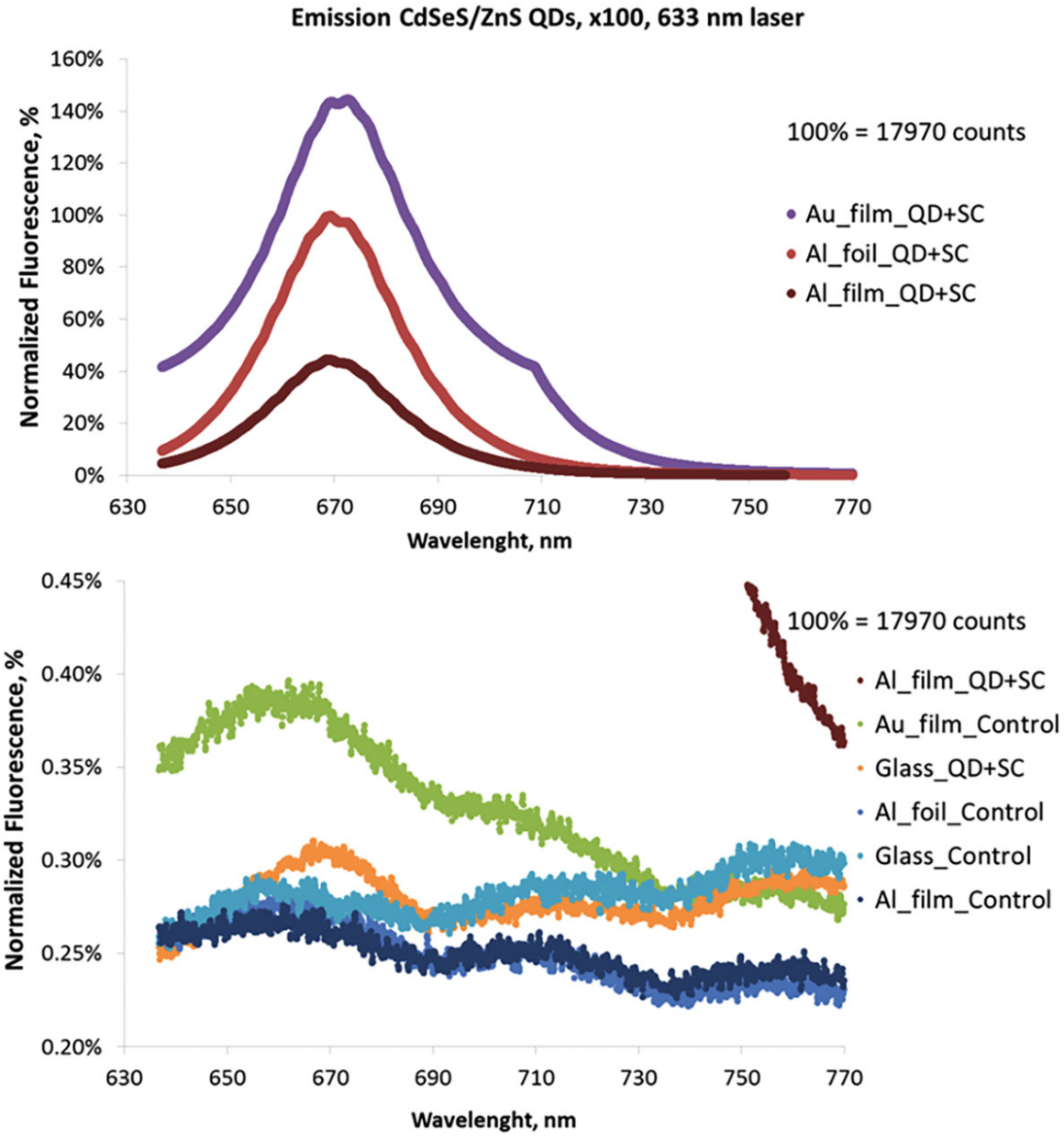

Figure 18. Averaged Normalized Fluorescence Emission spectra of CdSeS/ZnS QDs with single bacterial cells (QD + SC) and of control (just SC) on various substrates, obtained with 633 nm laser excitation wavelength and ×100 objective. Maximum intensity for averaged spectrum QD+SC on Al foil is set as 100% (17,970 counts).

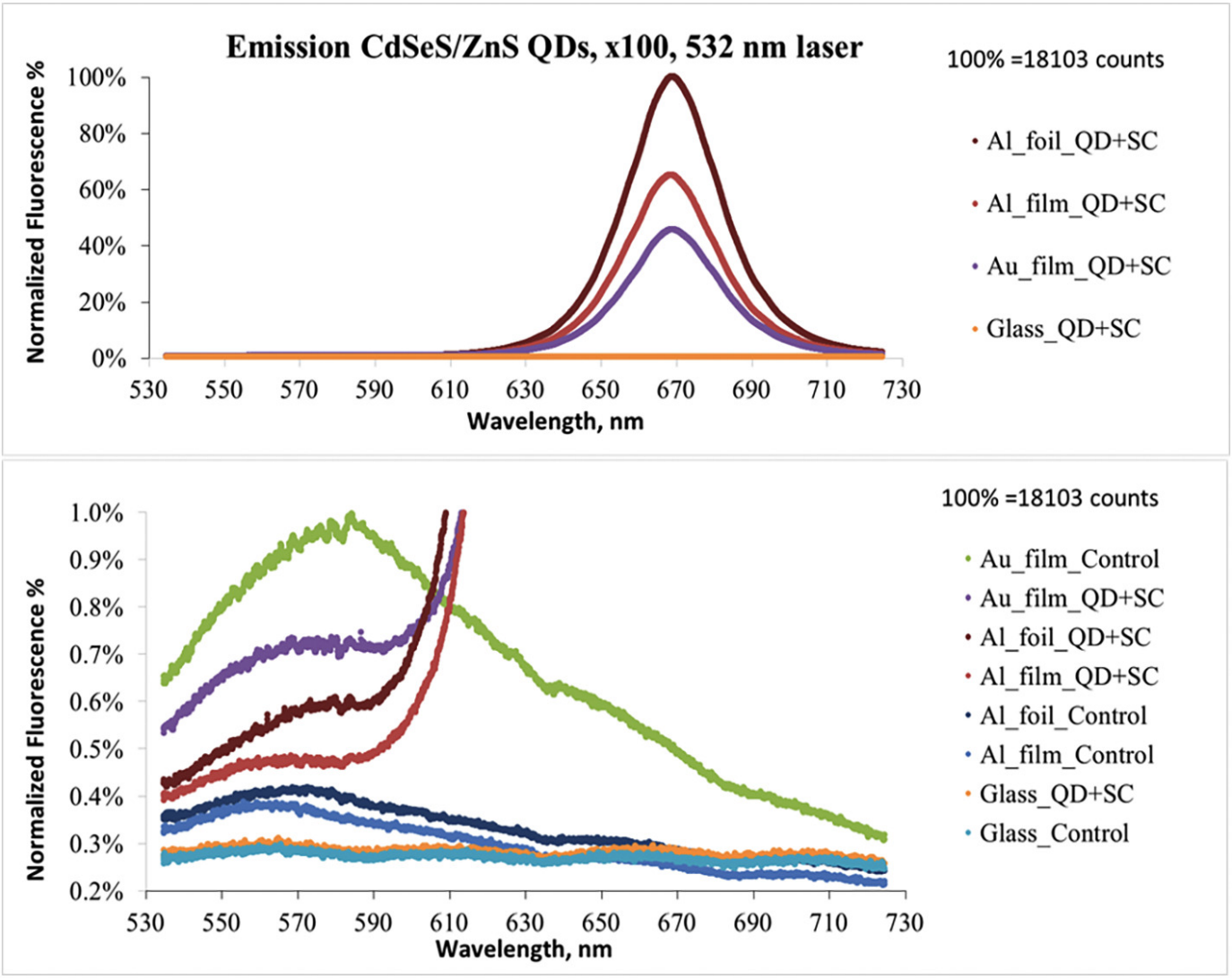

Figure 19. Averaged Normalized Fluorescence Emission spectra of CdSeS/ZnS QDs with single bacterial cells (QD + SC) and of control (just SC) on various substrates, obtained with 532 nm laser excitation wavelength and ×100 objective. Maximum intensity for averaged spectrum QD+SC on Al foil is set as 100% (18,103 counts).

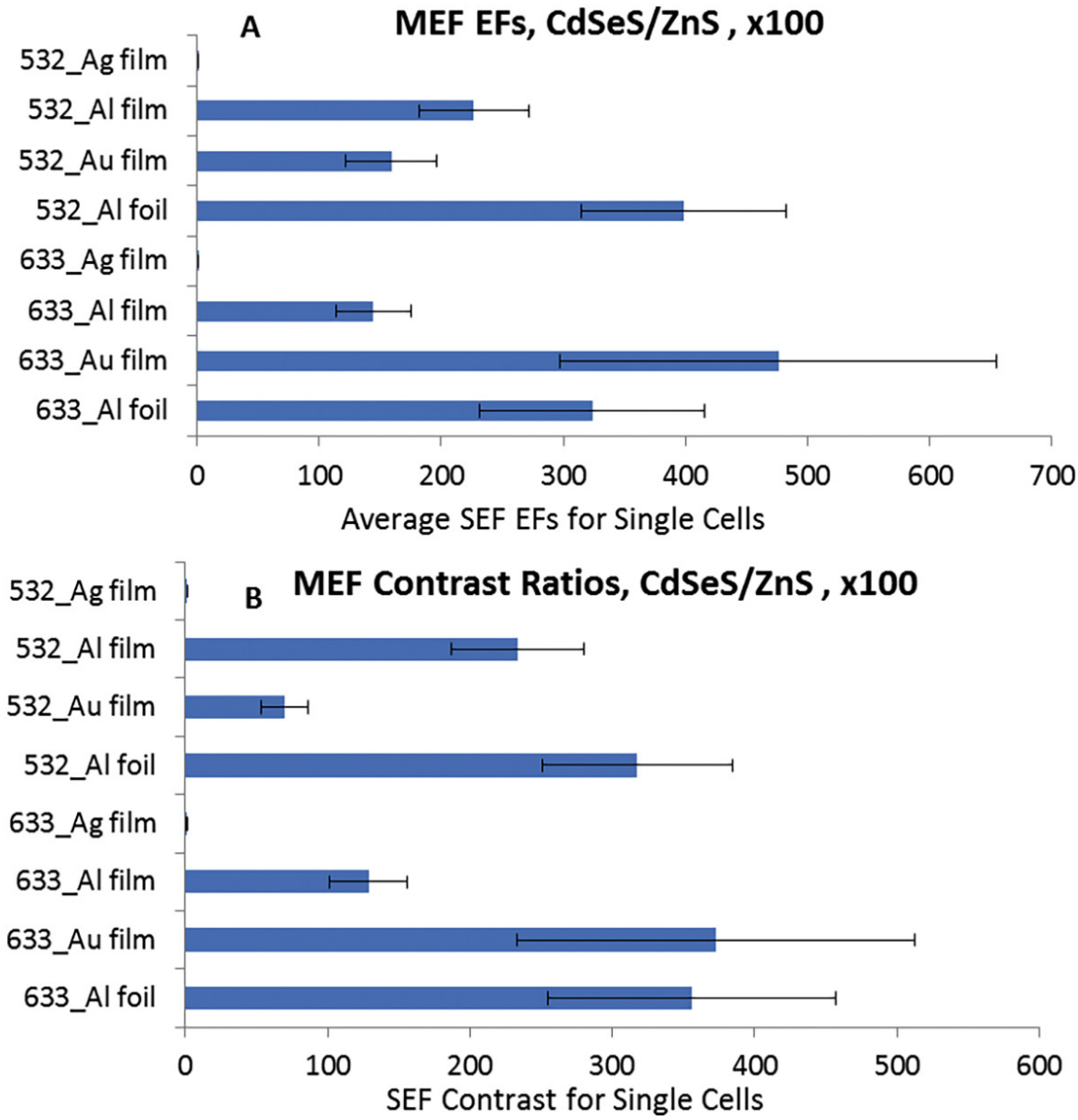

Figure 20. A) MEF Enhanced Factors calculated for CdSeS/ZnS QDs with single cells (×100 objective); B) MEF Contrast Ratios calculated for CdSeS/ZnS QDs with single cells on four substrates, ×100 objective. All EFs calculated as ratio of fluorescent signal on each of four substrates (silver, aluminum, gold films and aluminum foil) to signal on glass substrate. Contrast ratio is the maximum fluorescence intensity of QD labeled bacteria cells divided by maximum intensity of unlabeled (control) cell(s).

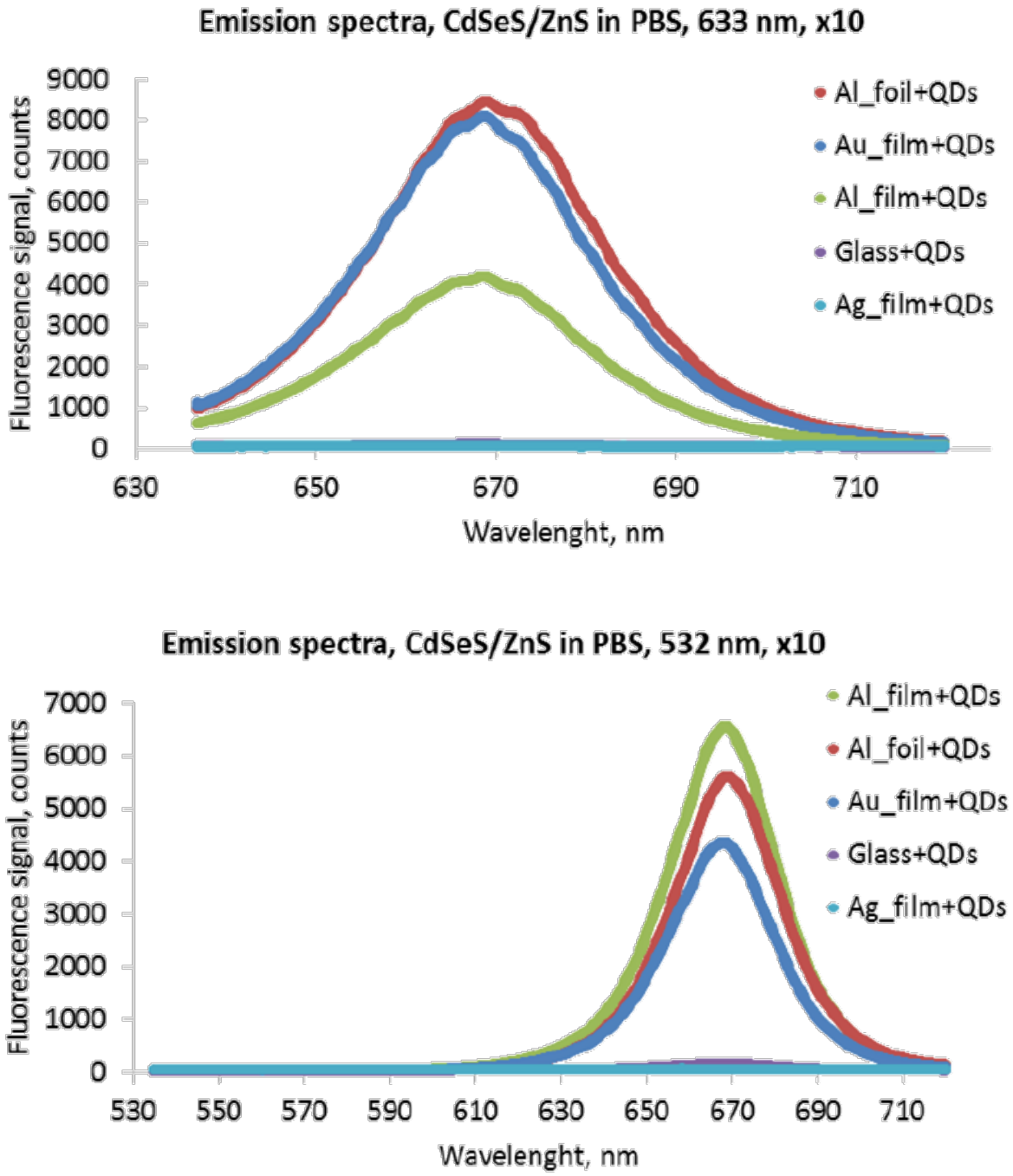

Figure 21. Averaged Normalized Fluorescence Emission spectra of CdSeS/ZnS QDs in PBS solution on various substrates, obtained with 633 and 532 nm laser excitation wavelength and x10 objective

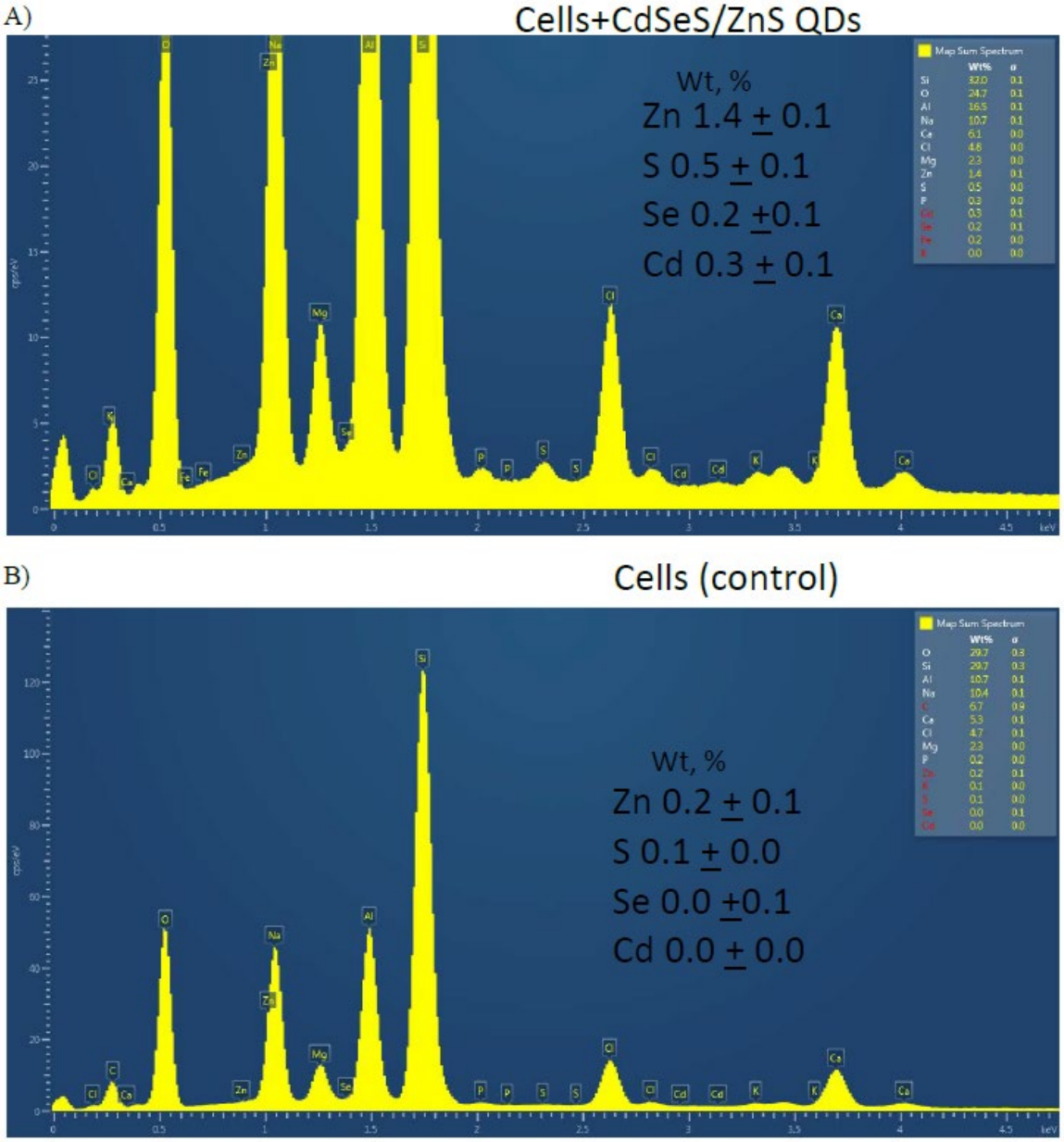

Figure 22. Representative EDS spectra on Al film: A) QD modified bacteria cells B) Control (No QDs)

excitation, those QDs in bacteria display the highest MEF enhancement factor relative to glass, as shown in the bar graph in Figure 20. The EF for QD + cells MEF on Al foil, on the other hand, is extremely high, exceeding 320. For MEF on Al foil, the maximum EF with a 532 nm laser was observed to be about 400 among three substrates. Overall, MEF is demonstrated on all three substrates (Au and Al films, Al foil) with the same 2+ order of magnitude enhancement. However, when comparing MEF emission on gold film to MEF emission on Al foil and Al film, Figure 20 shows that relative standard deviations in emission signal are on average around twice as high for MEF on a gold film. This observation can give Al foil a major advantage over the gold film as a MEF substrate because it is not only many times more affordable, but also, as far as we can tell, more reproducible.

Figure 20 shows that CdSeS/ZnS QDs with single bacterial cells have a fluorescence contrast ratio of at least two orders of magnitude for both excitation lasers 633 and 532 nm, or the ratio of signal from QD labeled cell(s) to signal from unlabeled/control cell(s). The maximum contrast on gold film and Al foil with 633 nm excitation are about 360–370, while the maximum contrast on Al film with the same laser is about 130. Al foil (317) has the highest contrast when excited with a 532 nm laser, whereas Al film (234) and gold have the lowest (69). As compared to the average for 532 nm excitation (207), the average maximum contrast for those three substrates is higher for 633 nm excitation (286). Moreover, the average enhancement factor is significantly higher for 633 nm excitation than for 532 nm excitation (315 vs 261, respectively). Thus, for this MEF method of single-cell + QDs observation, a 633 nm laser may be preferable to a 532 nm laser.

Because of the high contrast on each of those three metallic substrates, it should not be difficult to differentiate QD labeled cells from unlabeled cells using MEF of those non-

toxic QDs with a high degree of confidence, but this is not the case when the substrates are silver film or glass. Table 5 shows the contrast and EF values for all five substrates.

When we probed only CdSeS/ZnS and CdTe QDs in dried PBS solution on the surface of the same substrates, we found spectra with lower, but still important, EFs and lower contrasts for CdSeS/ZnS than bacteria cells labeled with the same QDs, as shown in Figure 21 and Table 5. The following are the general trends for bare QDs: With significant EFs around 40 at 633 nm excitation and EFs, around 20 at 532 nm excitation, Al foil, and Au film perform similarly. As those QDs enter the cell, their quenching by the metal surface is likely to be greatly reduced, and the emission rate tends to be increased by around one order of magnitude.

Also, from the EDS spectra in Figure 22, we can confirm the presence of CdSeS/ZnS QDs in the cells with the signal of three elements (Cd, S, and particularly Zn), with no significant presence of these elements in the control. But, the low concentration of QDs in cells makes this way of detection too unreliable for quantitative studies.

4.0 Conclusion

In this thesis, I demonstrated that the LOD of a biomarker in a sandwich SERS immunoassay on Si wafer is comparable or even lower than the LOD in the same assay on Au film. According to the conservative logarithmic calculation, the LODs for both substrates are around 30 pM. However, when calibrated with a four-parameter logistic model assay, silicon substrate outperforms gold film assays almost by an order of magnitude (LODs of 3 pM on silicon and 28 pM on gold). Furthermore, the silicon wafer substrate had lower relative and absolute standard deviations than the gold film. And the assay preparation took less than 24 hours and did not require expansive linker molecules. Because both lasers, 633 and 785 nm, delivered roughly the same LOD and minimum detectable concentrations for silicon as a substrate, as well as a similar dynamic range, we can assume that the assay on Si can also work in a relatively broad range of excitation wavelength.

In the SEF experiment, bacteria cells labeled with non-toxic CdSeS/ZnS QDs demonstrated very high SEF enhancement up to 450–480 on three substrates: Al foil, Al

film, Au film. And the SEF signals on Al foil and Al film were nearly twice as reproducible as the signal on Au film. However, silver film and CdTe QDs did not demonstrate any capabilities for fluorescence mapping of bacterial cells in any tests, which is explained by CdTe QDs' high cell toxicity and silver film's antimicrobial activity.

In the future, our research group plans to assess selectivity sandwich SERS immunoassay for different biomarkers, other than human and rat IgG. Also, we will try using other Raman reporters for this assessment. Particularly MPT64 a biomarker for tuberculosis, as Kazakhstan is currently considered high tuberculosis priority country and has the second-highest multidrug-resistant tuberculosis burden globally.[72-73]

Overall, both substrates showed comparable results to more widely accepted gold and silver substrates. Even though they are more cost-efficient and readily available, aluminum foil can even be bought in a nearby supermarket. Also, most importantly the results of these experiments showed that silicon wafer and aluminum foil can produce more reproducible signals than the gold film substrate. In the end, this thesis presented successful applications of simple and nontraditional aluminum foil and silicon wafer substrates in surface-enhanced Raman spectroscopy and surface-enhanced fluorescence.

5.0 References

1. Jeanmaire, D. L.; Van Duyne, R. P., Surface Raman spectroelectrochemistry Part I. Heterocyclic, aromatic, and aliphatic amines adsorbed on the anodized silver electrode. *Journal of Electroanalytical Chemistry* **1977,** *84* (1), 1-20.

2. Albrecht, M. G.; Creighton, J. A., Anomalously intense Raman spectra of pyridine at a silver electrode. *Journal of the American Chemical Society* **1977,** *99* (15), 5215-5217.

3. Wang, G.; Park, H.-Y.; Lipert, R. J.; Porter, M. D., Mixed Monolayers on Gold Nanoparticle Labels for Multiplexed Surface-Enhanced Raman Scattering Based Immunoassays. *Anal. Chem. (Washington, DC, U. S.)* **2009,** *81* (23), 9643-9650.

4. Schlucker, S., Surface-Enhanced Raman Spectroscopy: Concepts and Chemical Applications. *Angew Chem Int Edit* **2014,** *53* (19), 4756-4795.

5. Radziuk, D.; Moehwald, H., Prospects for plasmonic hot spots in single molecule SERS towards the chemical imaging of live cells. *Phys Chem Chem Phys* **2015,** *17* (33), 21072-21093.

6. Driscoll, A. J.; Harpster, M. H.; Johnson, P. A., The development of surface-enhanced Raman scattering as a detection modality for portable in vitro diagnostics: progress and challenges. *Phys Chem Chem Phys* **2013,** *15* (47), 20415-20433.

7. Song, J. B.; Huang, P.; Duan, H. W.; Chen, X. Y., Plasmonic Vesicles of Amphiphilic Nanocrystals: Optically Active Multifunctional Platform for Cancer Diagnosis and Therapy. *Accounts Chem Res* **2015,** *48* (9), 2506-2515.

8. Lane, L. A.; Qian, X. M.; Nie, S. M., SERS Nanoparticles in Medicine: From Label-Free Detection to Spectroscopic Tagging. *Chem Rev* **2015,** *115* (19), 10489-10529.

9. Grubisha, D. S.; Lipert, R. J.; Park, H. Y.; Driskell, J.; Porter, M. D., Femtomolar detection of prostate-specific antigen: An immunoassay based on surface-enhanced Raman scattering and immunogold labels. *Anal. Chem.* **2003,** *75* (21), 5936-5943.

10. Halvorson, R. A.; Vikesland, P. J., Surface-Enhanced Raman Spectroscopy (SERS) for Environmental Analyses. *Environ Sci Technol* **2010,** *44* (20), 7749-7755.

11. Nie, S.; Emory, S. R., Probing Single Molecules and Single Nanoparticles by Surface-Enhanced Raman Scattering. *Science* **1997,** *275* (5303), 1102-6.

12. Kneipp, K.; Wang, Y.; Kneipp, H.; Perelman, L. T.; Itzkan, I.; Dasari, R. R.; Feld, M. S., Single molecule detection using surface-enhanced raman scattering (SERS). *Physical Review Letters* **1997,** *78* (9), 1667-1670.

13. Camden, J. P.; Dieringer, J. A.; Wang, Y.; Masiello, D. J.; Marks, L. D.; Schatz, G. C.; Van Duyne, R. P., Probing the structure of single-molecule surface-enhanced Raman scattering hot spots. *J Am Chem Soc* **2008,** *130* (38), 12616-7.

14. Zhang, R.; Zhang, Y.; Dong, Z. C.; Jiang, S.; Zhang, C.; Chen, L. G.; Zhang, L.; Liao, Y.; Aizpurua, J.; Luo, Y.; Yang, J. L.; Hou, J. G., Chemical mapping of a single molecule by plasmon-enhanced Raman scattering. *Nature* **2013,** *498* (7452), 82-86.

15. Reverberi, R.; Reverberi, L., Factors affecting the antigen-antibody reaction. *Blood Transfus* **2007,** *5* (4), 227-40.

16. Hutter, E.; Fendler, J. H., Exploitation of localized surface plasmon resonance. *Adv Mater* **2004,** *16* (19), 1685-1706.

17. Bantz, K. C.; Meyer, A. F.; Wittenberg, N. J.; Im, H.; Kurtuluş, Ö.; Lee, S. H.; Lindquist, N. C.; Oh, S.-H.; Haynes, C. L., Recent progress in SERS biosensing. *Phys Chem Chem Phys* **2011,** *13* (24), 11551-11567.

18. Le Ru, E. C.; Galloway, C.; Etchegoin, P. G., On the connection between optical absorption/extinction and SERS enhancements. *Phys Chem Chem Phys* **2006,** *8* (26), 3083-3087.

19. Pilot, R.; Signorini, R.; Durante, C.; Orian, L.; Bhamidipati, M.; Fabris, L., A Review on Surface-Enhanced Raman Scattering. *Biosensors* **2019,** *9* (2), 57.

20. Stiles, P. L.; Dieringer, J. A.; Shah, N. C.; Van Duyne, R. R., Surface-Enhanced Raman Spectroscopy. *Annu Rev Anal Chem* **2008,** *1*, 601-626.

21. Langer, J.; Jimenez de Aberasturi, D.; Aizpurua, J.; Alvarez-Puebla, R. A.; Auguié, B.; Baumberg, J. J.; Bazan, G. C.; Bell, S. E. J.; Boisen, A.; Brolo, A. G.; Choo, J.; Cialla-May, D.; Deckert, V.; Fabris, L.; Faulds, K.; García de Abajo, F. J.; Goodacre, R.; Graham, D.; Haes, A. J.; Haynes, C. L.; Huck, C.; Itoh, T.; Käll, M.; Kneipp, J.; Kotov, N. A.; Kuang, H.; Le Ru, E. C.; Lee, H. K.; Li, J.-F.; Ling, X. Y.; Maier, S. A.; Mayerhöfer, T.; Moskovits, M.; Murakoshi, K.; Nam, J.-M.; Nie, S.; Ozaki, Y.; Pastoriza-Santos, I.; Perez-Juste, J.; Popp, J.; Pucci, A.; Reich, S.; Ren, B.; Schatz, G. C.; Shegai, T.; Schlücker, S.; Tay, L.-L.; Thomas, K. G.; Tian, Z.-Q.; Van Duyne, R. P.; Vo-Dinh, T.; Wang, Y.; Willets, K. A.; Xu, C.; Xu, H.; Xu, Y.; Yamamoto, Y. S.; Zhao, B.; Liz-Marzán, L. M., Present and Future of Surface-Enhanced Raman Scattering. *ACS Nano* **2020,** *14* (1), 28-117.

22. Phan, H. T.; Haes, A. J., What Does Nanoparticle Stability Mean? *The Journal of Physical Chemistry C* **2019,** *123* (27), 16495-16507.

23. Kleinman, S. L.; Frontiera, R. R.; Henry, A. I.; Dieringer, J. A.; Van Duyne, R. P., Creating, characterizing, and controlling chemistry with SERS hot spots. *Phys Chem Chem Phys* **2013,** *15* (1), 21-36.

24. Camden, J. P.; Dieringer, J. A.; Wang, Y.; Masiello, D. J.; Marks, L. D.; Schatz, G. C.; Van Duyne, R. P., Probing the structure of single-molecule surface-enhanced Raman scattering hot spots. *Journal of the American Chemical Society* **2008,** *130* (38), 12616-12617.

25. Zhang, X.; Young, M. A.; Lyandres, O.; Van Duyne, R. P., Rapid Detection of an Anthrax Biomarker by Surface-Enhanced Raman Spectroscopy. *Journal of the American Chemical Society* **2005,** *127* (12), 4484-4489.

26. Ma, K.; Yuen, J. M.; Shah, N. C.; Walsh, J. T.; Glucksberg, M. R.; Van Duyne, R. P., In Vivo, Transcutaneous Glucose Sensing Using Surface-Enhanced Spatially Offset Raman Spectroscopy: Multiple Rats, Improved Hypoglycemic Accuracy, Low Incident Power, and Continuous Monitoring for Greater than 17 Days. *Analytical Chemistry* **2011,** *83* (23), 9146-9152.

27. Sharma, B.; Frontiera, R. R.; Henry, A. I.; Ringe, E.; Van Duyne, R. P., SERS: Materials, applications, and the future. *Mater Today* **2012,** *15* (1-2), 16-25.

28. Willets, K. A., Super-resolution imaging of SERS hot spots. *Chemical Society Reviews* **2014,** *43* (11), 3854-3864.

29. Schumacher, L.; Jose, J.; Janoschka, D.; Dreher, P.; Davis, T. J.; Ligges, M.; Li, R.; Mo, M.; Park, S.; Shen, X.; Weathersby, S.; Yang, J.; Wang, X.; Meyer zu Heringdorf, F.; Sokolowski-Tinten, K.; Schlücker, S., Precision Plasmonics with Monomers and Dimers of Spherical Gold Nanoparticles: Nonequilibrium Dynamics at the Time and Space Limits. *The Journal of Physical Chemistry C* **2019,** *123* (21), 13181-13191.

30. Schlücker, S., Surface-Enhanced Raman Spectroscopy: Concepts and Chemical Applications. *Angewandte Chemie International Edition* **2014,** *53* (19), 4756-4795.

31. Porter, M. D.; Lipert, R. J.; Siperko, L. M.; Wang, G.; Narayanan, R., SERS as a bioassay platform: fundamentals, design, and applications. *Chemical Society Reviews* **2008,** *37* (5), 1001-1011.

32. Wang, G.; Lipert, R. J.; Jain, M.; Kaur, S.; Chakraboty, S.; Torres, M. P.; Batra, S. K.; Brand, R. E.; Porter, M. D., Detection of the Potential Pancreatic Cancer Marker MUC4 in Serum Using Surface-Enhanced Raman Scattering. *Analytical Chemistry* **2011,** *83* (7), 2554-2561.

33. Rye, H. S.; Dabora, J. M.; Quesada, M. A.; Mathies, R. A.; Glazer, A. N., Fluorometric Assay Using Dimeric Dyes for Double- and Single-Stranded DNA and RNA with Picogram Sensitivity. *Analytical Biochemistry* **1993,** *208* (1), 144-150.

34. Jablonski, A., Efficiency of Anti-Stokes Fluorescence in Dyes. *Nature* **1933,** *131* (3319), 839-840.

35. Strickler, S. J.; Berg, R. A., Relationship between Absorption Intensity and Fluorescence Lifetime of Molecules. *The Journal of Chemical Physics* **1962,** *37* (4), 814-822.

36. Ford, G. W.; Weber, W. H., Electromagnetic interactions of molecules with metal surfaces. *Physics Reports* **1984,** *113* (4), 195-287.

37. Chance, R. R.; Miller, A. H.; Prock, A.; Silbey, R., Fluorescence and energy transfer near interfaces: The complete and quantitative description of the Eu+3/mirror systems. *The Journal of Chemical Physics* **1975,** *63* (4), 1589-1595.

38. Moskovits, M., Surface-enhanced spectroscopy. *Reviews of Modern Physics* **1985,** *57* (3), 783-826.

39. Lakowicz, J. R., Radiative decay engineering 5: metal-enhanced fluorescence and plasmon emission. *Analytical biochemistry* **2005,** *337* (2), 171-194.

40. Wokaun, A., Surface-Enhanced Electromagnetic Processes. In *Solid State Physics*, Ehrenreich, H.; Turnbull, D.; Seitz, F., Eds. Academic Press: 1984; Vol. 38, pp 223-294.

41. Geddes, C. D.; Cao, H.; Gryczynski, I.; Gryczynski, Z.; Fang, J.; Lakowicz, J. R., Metal-Enhanced Fluorescence (MEF) Due to Silver Colloids on a Planar Surface: Potential Applications of Indocyanine Green to in Vivo Imaging. *The Journal of Physical Chemistry A* **2003,** *107* (18), 3443-3449.

42. Jeong, Y.; Kook, Y.-M.; Lee, K.; Koh, W.-G., Metal enhanced fluorescence (MEF) for biosensors: General approaches and a review of recent developments. *Biosensors and Bioelectronics* **2018,** *111*, 102-116.

43. Lakowicz, J. R.; Geddes, C. D.; Gryczynski, I.; Malicka, J.; Gryczynski, Z.; Aslan, K.; Lukomska, J.; Matveeva, E.; Zhang, J.; Badugu, R.; Huang, J., Advances in Surface-Enhanced Fluorescence. *Journal of Fluorescence* **2004,** *14* (4), 425-441.

44. Aslan, K.; Lakowicz, J. R.; Geddes, C. D., Metal-enhanced fluorescence using anisotropic silver nanostructures: critical progress to date. *Analytical and Bioanalytical Chemistry* **2005,** *382* (4), 926-933.

45. Lakowicz, J. R., Radiative Decay Engineering: Biophysical and Biomedical Applications. *Analytical Biochemistry* **2001,** *298* (1), 1-24.

46. Ray, K.; Chowdhury, M. H.; Lakowicz, J. R., Aluminum Nanostructured Films as Substrates for Enhanced Fluorescence in the Ultraviolet-Blue Spectral Region. *Analytical Chemistry* **2007,** *79* (17), 6480-6487.

47. Ray, K.; Szmacinski, H.; Lakowicz, J. R., Enhanced Fluorescence of Proteins and Label-Free Bioassays Using Aluminum Nanostructures. *Analytical Chemistry* **2009,** *81* (15), 6049-6054.

48. Akbay, N.; Lakowicz, J. R.; Ray, K., Distance-Dependent Metal-Enhanced Intrinsic Fluorescence of Proteins Using Polyelectrolyte Layer-by-Layer Assembly and Aluminum Nanoparticles. *The Journal of Physical Chemistry C* **2012,** *116* (19), 10766-10773.

49. Guerrini, L.; Graham, D., Molecularly-mediated assemblies of plasmonic nanoparticles for Surface-Enhanced Raman Spectroscopy applications. *Chem. Soc. Rev.* **2012,** *41* (21), 7085-7107.

50. Ishida, T.; Tsuneda, S.; Nishida, N.; Hara, M.; Sasabe, H.; Knoll, W., Surface-Conditioning Effect of Gold Substrates on Octadecanethiol Self-Assembled Monolayer Growth. *Langmuir* **1997,** *13* (17), 4638-4643.

51. Matikainen, A.; Nuutinen, T.; Itkonen, T.; Heinilehto, S.; Puustinen, J.; Hiltunen, J.; Lappalainen, J.; Karioja, P.; Vahimaa, P., Atmospheric oxidation and carbon contamination of silver and its effect on surface-enhanced Raman spectroscopy (SERS). *Scientific Reports* **2016,** *6*, 37192.

52. Knight, M. W.; King, N. S.; Liu, L.; Everitt, H. O.; Nordlander, P.; Halas, N. J., Aluminum for Plasmonics. *ACS Nano* **2014,** *8* (1), 834-840.

53. Gudun, K.; Elemessova, Z.; Khamkhash, L.; Ralchenko, E.; Bukasov, R., Commercial Gold Nanoparticles on Untreated Aluminum Foil: Versatile, Sensitive, and Cost-Effective SERS Substrate. *Journal of Nanomaterials* **2017,** *2017*, 8.

54. Mukanova, Z.; Gudun, K.; Elemessova, Z.; Khamkhash, L.; Ralchenko, E.; Bukasov, R., Detection of Paracetamol in Water and Urea in Artificial Urine with Gold Nanoparticle@Al Foil Cost-efficient SERS Substrate. *Analytical sciences : the international journal of the Japan Society for Analytical Chemistry* **2018,** *34* (2), 183-187.

55. Mogensen, K. B.; Gühlke, M.; Kneipp, J.; Kadkhodazadeh, S.; Wagner, J. B.; Espina Palanco, M.; Kneipp, H.; Kneipp, K., Surface-enhanced Raman scattering on aluminum using near infrared and visible excitation. *Chemical Communications* **2014,** *50* (28), 3744-3746.

56. Jiang, Z.; Xiangxu, J.; Su, S.; Wei, X.; Lee, S.; He, Y., Silicon-based reproducible and active surface-enhanced Raman scattering substrate for sensitive, specific and multiplex DNA detection. *Applied Physics Letters* **2012,** *100*.

57. Kosović, M.; Balarin, M.; Ivanda, M.; Đerek, V.; Marciuš, M.; Ristić, M.; Gamulin, O., Porous Silicon Covered with Silver Nanoparticles as Surface-Enhanced Raman Scattering (SERS) Substrate for Ultra-Low Concentration Detection. *Applied spectroscopy* **2015,** *69*.

58. Upender, G.; Sathyavathi, R.; Raju, B.; Bansal, C.; Narayana Rao, D., SERS study of molecules on Ag nanocluster films deposited on glass and silicon substrates by cluster deposition method. *Journal of Molecular Structure* **2012,** *1012*, 56-61.

59. Edwards, P. P.; Porch, A.; Jones, M. O.; Morgan, D. V.; Perks, R. M., Basic materials physics of transparent conducting oxides. *Dalton Transactions* **2004,** (19), 2995-3002.

60. Choi, S.; Chae, J., Methods of reducing non-specific adsorption in microfluidic biosensors. *Journal of Micromechanics and Microengineering* **2010,** *20* (7), 075015.

61. Sultangaziyev, A.; Bukasov, R., Review: Applications of surface-enhanced fluorescence (SEF) spectroscopy in bio-detection and biosensing. *Sensing and Bio-Sensing Research* **2020,** *30*, 100382.

62. Kunushpayeva, Z.; Rapikov, A.; Akhmetova, A.; Sultangaziyev, A.; Dossym, D.; Bukasov, R., Sandwich SERS immunoassay of human immunoglobulin on silicon wafer compared to traditional SERS substrate, gold film. *Sensing and Bio-Sensing Research* **2020,** *29*, 100355.

63. Holstein, C. A.; Griffin, M.; Hong, J.; Sampson, P. D., Statistical Method for Determining and Comparing Limits of Detection of Bioassays. *Analytical Chemistry* **2015,** *87* (19), 9795-9801.

64. Zhu, H.; Sikora, U.; Ozcan, A., Quantum dot enabled detection of Escherichia coli using a cell-phone. *Analyst* **2012,** *137* (11), 2541-2544.

65. O'Connell, M. A.; Belanger, B. A.; Haaland, P. D., Calibration and assay development using the four-parameter logistic model. *Chemometrics and Intelligent Laboratory Systems* **1993,** *20* (2), 97-114.

66. Sergiienko, S.; Moor, K.; Gudun, K.; Yelemessova, Z.; Bukasov, R., Nanoparticle–nanoparticle vs. nanoparticle–substrate hot spot contributions to the SERS signal: studying Raman labelled monomers, dimers and trimers. *Phys Chem Chem Phys* **2017,** *19* (6), 4478-4487.

67. Fu, Y.; Kim, D.; Jiang, W.; Yin, W.; Ahn, T. K.; Chae, H., Excellent stability of thicker shell CdSe@ZnS/ZnS quantum dots. *RSC Advances* **2017,** *7* (65), 40866-40872.

68. Li, Z.; Dong, C.; Tang, L.; Zhu, X.; Chen, H.; Ren, J., Aqueous synthesis of CdTe/CdS/ZnS quantum dots and their optical and chemical properties. *Luminescence* **2011,** *26* (6), 439-448.

69. Jaiswal, J. K.; Mattoussi, H.; Mauro, J. M.; Simon, S. M., Long-term multiple color imaging of live cells using quantum dot bioconjugates. *Nature Biotechnology* **2003,** *21* (1), 47-51.

70. Fang, T.-T.; Li, X.; Wang, Q.-S.; Zhang, Z.-J.; Liu, P.; Zhang, C.-C., Toxicity evaluation of CdTe quantum dots with different size on Escherichia coli. *Toxicology in Vitro* **2012,** *26* (7), 1233-1239.

71. Choi, Y.; Kim, H.-A.; Kim, K.-W.; Lee, B.-T., Comparative toxicity of silver nanoparticles and silver ions to Escherichia coli. *Journal of Environmental Sciences* **2018,** *66*, 50-60.

72. Hermosilla, S.; You, P.; Aifah, A.; Abildayev, T.; Akilzhanova, A.; Kozhamkulov, U.; Muminov, T.; Darisheva, M.; Zhussupov, B.; Terlikbayeva, A.; El-Bassel, N.; Schluger, N., Identifying risk factors associated with smear positivity of pulmonary tuberculosis in Kazakhstan. *PLOS ONE* **2017,** *12* (3), e0172942.

73. Jørstad, M. D.; Marijani, M.; Dyrhol-Riise, A. M.; Sviland, L.; Mustafa, T., MPT64 antigen detection test improves routine diagnosis of extrapulmonary tuberculosis in a low-resource setting: A study from the tertiary care hospital in Zanzibar. *PLOS ONE* **2018,** *13* (5), e0196723.